A rotating smeared crack approach in Sequentially Linear Analysis using the Elastic-brittle fraction model

Bresser, D.; Rots, J. G.; Hendriks, M. A.N.; Pari, M.

DOI
10.1016/j.engfracmech.2022.108953

Publication date
2023

Document Version
Final published version

Published in
Engineering Fracture Mechanics

Engineering Fracture Mechanics 277 (2023) 108953

Contents lists available at ScienceDirect

Engineering Fracture Mechanics

journal homepage: www.elsevier.com/locate/engfracmech

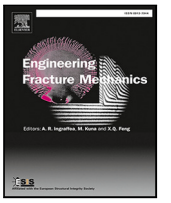

A rotating smeared crack approach in Sequentially Linear Analysis using the Elastic-brittle fraction model

D. Bresser [a], J.G. Rots [a], M.A.N. Hendriks [a,b], M. Pari [a,*]

[a] Faculty of Civil Engineering and Geosciences, Delft University of Technology, P.O. Box 5048, 2600 GA Delft, The Netherlands
[b] Norwegian University of Science and Technology (NTNU), Rich. Birkelandsvei 1A, 7491 Trondheim, Norway

ARTICLE INFO

Keywords:
Sequentially Linear Analysis (SLA)
Quasi-brittle materials
Rotating smeared crack model
Fraction model
Orthotropic damage
Nonlinear softening

ABSTRACT

Sequentially Linear Analysis (SLA), an event-by-event solution strategy in which a sequence of scaled linear analyses with decreasing secant stiffness is performed, representing local damage increments; is a robust alternative to nonlinear finite element analysis of quasi-brittle structures. Since it is based on a fixed smeared crack constitutive model, severe spurious stresses and inaccuracies may develop due to misalignment of the crack with the principal stress directions. To this end, the elastic-brittle fraction model was conceived. The model separates the continuum into several parallel fractions or layers, each with different properties, chosen in order to represent the overall constitutive softening behaviour as accurately as possible. The main idea is to mimick a rotating crack by a superposition of fractions, each with a fixed crack direction. In this article, the model is presented for both the 2-dimensional and 3-dimensional frameworks, with a general transition from any saw-tooth law to fraction material properties. The fraction models are then validated and compared against the fixed crack model with SLA: using single element and structural case studies. It is shown that the fraction model is able to mimick the rotating crack model, that it leads to lesser spurious cracks and narrower localisation bands, and in turn results in a more flexible post-peak response over all case studies compared to the fixed crack model.

1. Introduction

For centuries, quasi-brittle materials like concrete and masonry have been prevalently used as building material in the construction industry. Concrete is used for its high compressive strength and favourable durability [1]. However, the material entails some significant drawbacks: concrete has a small tensile load-bearing capacity and shows quasi-brittle fracture behaviour, meaning that after the initiation of damage only a relatively small residual deformation capacity is available. Hence, the structure cracks quite abruptly and very locally, and these cracks induce peaky behaviour in the load–displacement curve. Around these peaks, standard incremental iterative analysis, also called Non-Linear Finite Element Analysis (NLFEA), shows convergence problems due to the origin of alternative equilibrium paths. Consequently, the robustness of the solution procedure is strongly affected by quasi-brittle fracture, as has been found by many authors [2–4]. Within the framework of smeared cracking, as pioneered by Rashid [5] and later on improved by Bazant and Oh [6], many advanced solution methods have been proposed over the years to tackle these convergence issues, e.g. arc-length control [7] and energy release control [8]. Despite the numerous proposed solutions, robustness of incremental iterative analysis for quasi-brittle materials remains a topic of research, especially regarding the analysis of full-scale structures in engineering practice.

* Corresponding author.
E-mail address: M.Pari@tudelft.nl (M. Pari).

https://doi.org/10.1016/j.engfracmech.2022.108953
Received 26 July 2022; Received in revised form 21 October 2022; Accepted 16 November 2022
Available online 25 November 2022

These convergence issues can be inherently circumvented by invoking linear event-by-event approaches, providing a more robust alternative. Inspired by so-called lattice models [9–11], in which a continuum is modelled by a network of elastic truss or beam elements, Rots [12–14] proposed the framework of *Sequentially Linear Analysis*, from now on abbreviated by SLA. SLA is an event-by-event strategy based on the fixed smeared cracking model, in which a sequence of scaled linear analyses with a decreasing secant stiffness is performed, representing local damage increments. The continuous stress–strain softening curve is replaced by a discontinuous saw-tooth curve. Instead of increasing the load on a structure, the approach locally increases the damage of the considered structure, such that no abrupt cracks are missed and the complete load–displacement path is obtained from the damage driven process. During the last decade, many research studies have been performed on SLA. The saw-tooth model has been improved to make the fracture energy independent of the number of saw-teeth [14]. The method has been proven to be an alternative for structural applications in masonry [15] and glass [16]. Extensions towards non-proportional loading within the framework of SLA have been developed [17–19]. Additionally, a Force-release method has been proposed [20] to incorporate non-proportional loading, in which unbalance stresses are gradually redistributed after each damage increment, potentially inducing new events. Influences of mesh-directional bias have been reduced by the determination of smoothly curved C^1-continuous crack paths [21], and a multi-surface constitutive model for interface elements suitable for discrete modelling of damage in masonry and concrete has also been proposed [22]. Furthermore, SLA has been combined with incremental iterative analysis [23], combining the advantages of both approaches. In order to apply SLA to real-life structures, the approach has been extended towards shell elements [24], 3D-elements [25], including non-proportional loading as well, and efficient linear solvers have been proposed to improve the speed of SLA [26].

The current SLA-framework is based on a fixed cracking model, in which the direction of a crack is fixed upon damage initiation, potentially causing the development of severe spurious stresses and inaccuracies due to the misalignment of the crack with the principal stress directions [2,27,28]. These spurious stresses cause additional energy dissipation and as a result, the structure behaves stiffer, which is also referred to as stress-locking effects. In an attempt to mimick rotating cracks within sequentially linear analysis, Hendriks and Rots [29] proposed a model consisting of several parallel fractions or layers, from now on called the *Elastic-brittle fraction model*. Each of these fractions is elastic-perfectly brittle, but has different properties, chosen such to represent the constitutive behaviour as accurately as possible. The fractions fail independent of each other and have their own specific crack direction. The main idea is to mimick a rotating crack by a superposition of fractions each having their own fixed crack direction, thereby reducing the aforementioned development of spurious stresses. The first test results are promising [29]: no over-stiff behaviour of the model is observed, thus indicating similarities to a rotating crack model. The elastic-brittle fraction model fits well within the framework of SLA and, since the model has not been fully developed yet and is only tested for a limited number of cases, this study will proceed on the work of Hendriks and Rots.

In this study, the frameworks of regular SLA and the elastic-brittle fraction model are connected by a general transition from any saw-tooth law to fraction material properties, thereby generalising the approach. Furthermore, the 2-dimensional framework of the fraction model has been extended towards 3-dimensional structures to broaden the range of applications. Both the 2D and 3D frameworks are based on a smeared cracking model invoking an orthogonal damage approach, restricted to mode I tension softening for homogeneous quasi-brittle materials, as described by the fictitious crack model [30]. Although compressive crushing is not considered, the same approach can be applied for those cases as well. The article is organised as follows. Firstly, the current framework of SLA is elaborated and the motivation for a rotating crack approach in SLA is substantiated. Secondly, the framework and the work flow of the elastic-brittle fraction model are formally described for both 2D and 3D. Next, validation studies against experimental benchmarks are performed and the fractions are indeed proved to crack sequentially under slightly different angles approximating a rotating crack model, thereby significantly reducing the stiffening effects of spurious stresses.

2. SLA - methodology

For the simplified case of proportional loading, the following procedure is used in sequentially linear analysis:

- Add the external load as a reference unit load.
- Perform a linear elastic analysis and determine the principal stresses in all integration points.
- Determine the critical integration point in the structure, which is the integration point for which the principal stress utilises most of the current strength capacity of that specific point.
- Determine the critical load multiplier, which is the ratio between the strength and the stress in the critical integration point, and scale the reference load proportionally. Subsequently, determine the stress and strain fields by multiplying the unit load response with the critical load multiplier.
- Perform a damage increment by reducing the strength and stiffness of the critical integration point according to a predefined saw-tooth constitutive law, which will be discussed later in this section.
- Repeat this cycle of steps until the damage has reached a user-specified state. The non-linear response can be constructed by connecting all consecutively found linear responses.

For the more complicated case of non-proportional loading paths, the main concept of the approach remains the same, although the reader is referred to Refs. [17–19] for more information. Since the procedure damages a unique critical point one by one, it avoids multiple cracks to occur simultaneously as in the incremental-iterative procedure, thereby circumventing alternate equilibrium paths or bifurcations points.

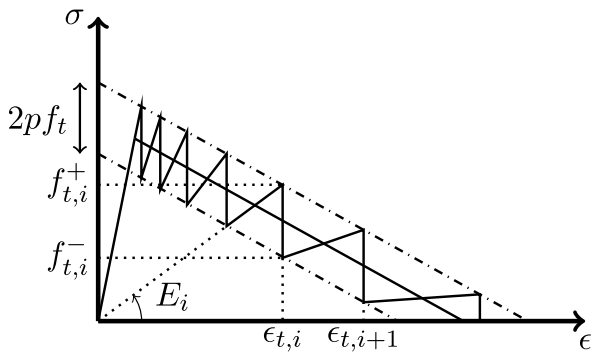

Fig. 1. Transition from continuum constitutive law (linear tension softening) to a ripple band saw-tooth law.

Within the framework of SLA, nonlinear constitutive laws are approximated with the aid of step-wise secant materials laws, in literature often called saw-tooth laws. These laws prescribe the reduction of the strength and stiffness at each damage increment. During the last two decades, different types of saw-tooth formulations have been developed [12–14,18]. In this study, the ripple band formulation [14] is applied, as this formulation ensures the dissipated energy (or fracture energy) to be independent of the mesh-size. In the ripple band formulation, a strength range is set as a percentage p of the maximum tensile strength. Two auxiliary curves are drawn: one $+pf_t$ above and one $-pf_t$ below the continuum constitutive curve, defining an envelope around the softening curve, as visualised by Fig. 1 for the case of linear tension softening. First, the point of intersection $\epsilon_{t,i}$ between the secant elastic branch with stiffness E_i and the upper curve is determined. The corresponding stress is called $f^+_{t,i}$. Then, the tensile strength $f^-_{t,i}$ on the bottom curve for the same strain $\epsilon_{t,i}$ is calculated and based on that, the new reduced secant stiffness E_{i+1} for the next saw-tooth is obtained by

$$E_{i+1} = \frac{f^-_{t,i}}{\epsilon_{t,i}} \tag{1}$$

with

$$f^-_{t,i} = f^+_{t,i} - 2pf_t \tag{2}$$

This procedure is repeated until a stress-free state is reached, equivalent to a fully developed crack. The number of saw-teeth N follows from the procedure and depends on the width of the ripple band $2pf_t$.

In this study, the procedure is applied in the context of a total strain based smeared cracking model. Upon crack initiation, the initial isotropic stress–strain relation is replaced by an orthotropic relation, in line with the orthotropic damage model, and the axes of orthotropy (normal direction n and tangential direction t) are determined by the principal stress directions at crack initiation. As the current framework of SLA is based on a fixed crack model, the axes of orthotropy are fixed upon crack initiation. For plane stress states, the orthotropic constitutive relation is given by (e.g. [17,18]):

$$\begin{bmatrix}\sigma_{nn}\\ \sigma_{tt}\\ \sigma_{nt}\end{bmatrix} = \frac{1}{1-\nu_{tn}\nu_{nt}}\begin{bmatrix}E_n & \nu_{nt}E_n & 0\\ \nu_{tn}E_t & E_t & 0\\ 0 & 0 & \left(1-\nu_{tn}\nu_{nt}\right)G_{red}\end{bmatrix}\begin{bmatrix}\epsilon_{nn}\\ \epsilon_{tt}\\ \gamma_{nt}\end{bmatrix} \tag{3}$$

where E_n, E_t, G_{red}, ν_{nt} and ν_{tn} are the damaged apparent properties. After the formation of a primary crack, the direction of the crack is fixed and a reduced normal stiffness E_n is inserted according to the applied saw-tooth law and E_t remains E_0, as this direction is yet uncracked. Within the considered model, a second crack is allowed to form perpendicular to the primary crack. Then, the tangential stiffness E_t is also reduced according to the predefined saw-tooth law. The Poisson's ratios are assumed to reduce accordingly with the modulus of elasticity:

$$\nu_{nt} = \nu_0\frac{E_t}{E_0} \quad \text{and} \quad \nu_{tn} = \nu_0\frac{E_n}{E_0} \tag{4}$$

where ν_0 and E_0 are the initial Poisson's ratio and stiffness. For fixed crack models, the definition of a saw-tooth law for E_n and E_t is not sufficient, as the principal directions might start to deviate from the crack direction introducing shear stresses on the cracking plane. Hence, also the development of shear stresses and especially the shear stiffness G_{red} during cracking must be considered. In this study, the shear retention relation as proposed in the work of DeJong et al. [17] is applied:

$$G_{red} = \frac{E_{min}}{2\left(1+\nu_0\frac{E_{min}}{E_0}\right)} = \beta G_0 \tag{5}$$

where $E_{min} = \min(E_n, E_t)$, β is the shear retention factor and G_0 the initial shear modulus of the material.

3. Motivation for rotating crack approach in SLA

The axes of orthotropy, which describe the cracking plane, are fixed upon crack initiation within a fixed crack model. However, during further loading, the principal stress directions might change as a result of e.g. changing load conditions (non-proportional loading) and stress redistribution during the fracture process. Due to the crack not co-rotating with the principal stress directions, shear stresses are generated within the cracking plane, which is troubling for two reasons:

1. Stresses larger than the tensile strength can occur unnoticed as only the stresses along the fixed axes of orthotropy are monitored, whereas the actual principal stress directions should be monitored to find the maximum stresses. In this way, *stress locking* takes place, meaning that non-physical stresses, also known as spurious stresses, are generated within the cracking plane leading to an incorrect over-stiff structural behaviour, especially when smeared cracks have to propagate in a zig-zag fashion through the mesh.
2. In order to more realistically represent the stress rotations within the fixed crack model, the shear retention relation, as given by Eq. (5), can be adapted. However, this inevitably leads to more complicated material laws or additional material properties [31], which is not desirable for application in engineering practice.

The current SLA framework is based on a fixed crack model. Within a rotating crack model, the crack directions co-rotate with the principal stress directions such that the development of spurious stresses is avoided. To this end, the unfavourable effects of stress locking on SLA are expected to reduce for a rotating crack approach in SLA. Stress locking also results from the inability of finite elements to reproduce the discontinuous nature of the actual displacement field around a crack [32]. This type of stress locking is not expected to reduce for a rotating crack approach in SLA. Since SLA is an event-by-event strategy, in which each event influences the subsequent events, it is expected that a rotating crack approach in SLA does not merely influence the local fracture behaviour (e.g. less stress locking), but also affects the global fracture behaviour by more accurate crack paths and better crack localisation.

For these reasons, several researchers [27,31,33,34] tried to envisage a rotating crack model within an event-by-event strategy like SLA. By definition, an event-by-event strategy can only update 1 integration point at a time, whilst the rotating crack model requires the crack directions of all cracked integration points to be updated during each event. Furthermore, the rotation of the principal stresses and strains is non-linearly related to the load multiplier [27] and therefore, the nature of a rotating crack model does not directly suit SLA. In literature, four alternative models are available to incorporate the rotation of cracks in SLA, which are briefly discussed underneath (for more information, the reader is referred to the given references).

- **Rotating crack as an event:** one way of implementing rotating cracks within the framework of SLA is to define a new type of event: the rotation of a crack, which is performed once a certain threshold angle is reached between the cracking plane and the actual principal directions (only for cracked integration points). This approach has been elaborated by Slobbe [33] assuming only proportional loading on the structure. The approach suffers from the so-called 'snowball-effect': a crack rotation event causes a change in stiffness and thereby a local stress redistribution, which in its turn again induces a crack rotation, a subsequent change in stiffness and so on.
- **Rotating crack in a Force-Release strategy:** following a different path, Vorel and Boshoff [27] developed a rotating crack model that can be used within the framework of SLA to analyse the behaviour of composites. As a starting point, the Force-Release (F-R) approach [20], an incremental version of SLA, is utilised, in which the unbalanced forces are gradually redistributed, with the possibility to induce another event meanwhile. The principal direction of the critical integration point is updated after each stress redistribution. As the rotation of the principal directions is not known beforehand and depends on the scaling factor, it is assumed that the load multiplier can be evaluated with respect to the last equilibrated principal direction of the considered integration point. It is noted that the approach is not merely a secant linear analysis anymore, as the disbalance forces are redistributed with the aid of load increments, hence following an incremental type of approach. The method has been applied to a three-point bending test in shear failure and in bending failure. For both cases, the adapted version of SLA including rotating cracks gave similar load displacement curves as the experiment and an incremental iterative analysis.
- **Rotating crack as a multi-directional crack:** Lately, another approach to simulate a rotating crack model within SLA was developed by Cook et al. [31]. Although the approach is developed for a different field of application, namely heterogeneous brittle materials on a micro scale (aggregate grain level), it is also applicable for computational modelling of concrete structures. In this approach, which is in fact a multi-directional smeared fixed crack approach, each element is given a certain amount of predefined potential cracking planes. With the aid of a sequentially linear analysis, the critical potential crack plane is searched for and damage increments are performed within the critical crack plane. The approach differs from SLA in the sense that a critical pre-defined crack plane is searched for instead of a critical integration point. By allowing multiple fixed cracks to form within one element in combination with a crack-tracking algorithm, rotating cracks are successfully simulated and stress locking effects are reduced by the approach.
- **Rotating crack in a sub-element strategy:** Recently, a study by Liu [34] has been published, proposing a so-called sub-element strategy, in which an element is discretised into elastic-perfectly brittle overlay elements. Although the author does not mention this in their work, clear similarities with the fraction model [29] are found. However, the sub-element model is more or less applied as a lattice model and no attention is paid to the crack direction. The main purpose of the sub-element model by Liu was to offer an alternative to incremental iterative analysis and regular SLA, although it is fundamentally similar to the fraction model and could have been used to mimick a rotating crack model as well.

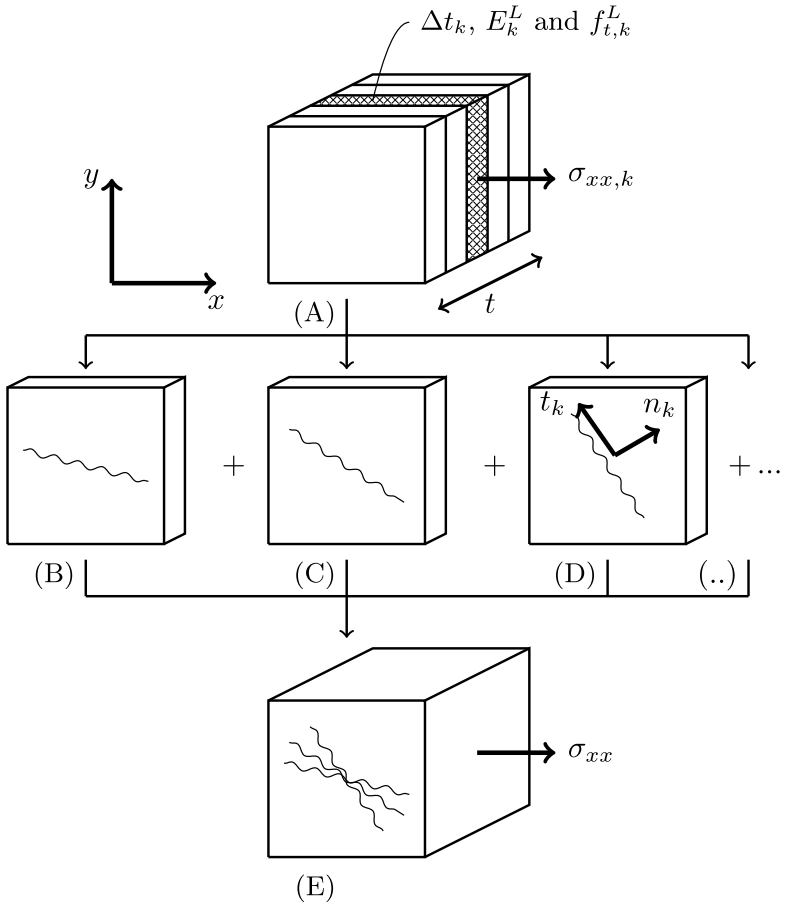

Fig. 2. (A) Single element elastic-brittle fraction model with definitions of fraction properties; (B)–(C)–(D)–(..) the fractions with each of their own fixed crack directions and (E) the total element mimicking a rotating crack.

4. Elastic-brittle fraction model and work flow

In an attempt to mimick the effects of rotational cracking within sequentially linear analysis, Hendriks and Rots [29] developed the *Elastic-brittle fraction model*. In two-dimensional space, this model subdivides each element in a set of N parallel fractions k, as visualised in Fig. 2(A). Each of these fractions is elastic-perfectly brittle with tensile strength $f_{t,k}$, compressive strength $f_{c,k}$, stiffness E_k and thickness Δt_k, chosen in order to represent the continuum constitutive material law as accurately as possible. The Poisson's ratio ν_k is the same for all fractions and equal to the material property ν. The total behaviour is found by the superposition of the stresses and strains of the perfectly brittle fractions in parallel. Each of the fractions is allowed to have its own crack direction θ_k and therefore, the global/overall crack direction might rotate. In other words, the model utilises a fixed cracking model per fraction and mimicks a rotating crack on element level. This process is depicted by Fig. 2, where (B)–(D) are the fixed crack fractions and (E) is the mimicked rotating crack. Because the crack on element level is allowed to rotate, the proposed model might potentially reduce stress locking effects, as briefly touched upon in Section 3.

As mentioned by Hendriks and Rots, the model describes softening as a gradual reduction of the cross-sectional area. In fact, this is a more physically justified approach compared to regular SLA, as the formation of micro-cracks in the fracture zone, according to the fictitious crack model of Hillerborg et al. [30], is equivalent to a reduction of the effective material cross-section. In the following section, the theoretical framework of the elastic-brittle fraction model will be further elaborated for both 2D and 3D. As the 3-dimensional framework is similar to its 2-dimensional equivalent, the elaboration of the 3-dimensional framework is limited.

4.1. 2-dimensional framework

4.1.1. Elastic-brittle constitutive relation per fraction and superposition

On a fraction level, represented by Figs. 2(B)–(D), the constitutive behaviour is governed by a fixed cracking approach. Therefore, the theory as discussed in Section 2 can be applied straightforwardly. For a parallel fraction k, the elastic-perfectly brittle material

behaviour is shown by Fig. 3(B). Up until either the compressive or tensile strength is reached, the fractions behave isotropic according to

$$\begin{bmatrix}\sigma_{xx}\\ \sigma_{yy}\\ \sigma_{xy}\end{bmatrix}_k = \frac{E_k}{1-\nu_k^2}\begin{bmatrix}1 & \nu_k & 0\\ \nu_k & 1 & 0\\ 0 & 0 & \frac{1-\nu_k}{2}\end{bmatrix}\begin{bmatrix}\epsilon_{xx}\\ \epsilon_{yy}\\ \gamma_{xy}\end{bmatrix} \tag{6}$$

where E_k and ν_k are the fractions' stiffness and Poisson's ratio respectively. The strain vector does not have an index k as the strain is the same for all fractions. Once the tensile or compressive strength is reached in direction n_k (the maximum stress is obtained in the principal stress direction), a completely developed crack perpendicular to the failure stress in direction t_k is formed and the stiffness $E_{n,k} = 0$ is completely lost, representing the brittleness of the fraction. This is followed by the orthotropic material behaviour. The principal stresses $\sigma_{nn,k}$ and $\sigma_{tt,k}$ are found using the Mohr's circle:

$$\sigma_{nn,tt,k} = \frac{\sigma_{xx,k}+\sigma_{yy,k}}{2} \pm \sqrt{\left(\frac{\sigma_{xx,k}-\sigma_{yy,k}}{2}\right)^2 + \sigma_{xy,k}^2} \tag{7}$$

The crack direction θ_k is fixed to the principal stress and strain directions just before cracking, which coincide due to the isotropic behaviour prior to cracking. From Mohr's circle:

$$\tan(2\theta_k) = \frac{2\sigma_{xy,k}}{\sigma_{xx,k}-\sigma_{yy,k}} = \frac{\gamma_{xy}}{\epsilon_{xx}-\epsilon_{yy}} \tag{8}$$

where the stresses and strains prior to crack formation are used. As the stiffness $E_{n,k}$ is completely lost, the Poisson's ratio ν_{tn} reduces according to Eq. (4) to 0. The crack is completely developed, meaning that no shear stresses are transmitted within the cracking plane. Eq. (5) gives $G_{red} = 0$, meaning that zero shear retention is obtained. Hence, the orthotropic fixed smeared crack formulation of Eq. (6) reduces to

$$\begin{bmatrix}\sigma_{nn}\\ \sigma_{tt}\\ \sigma_{nt}\end{bmatrix}_k = \begin{bmatrix}0 & 0 & 0\\ 0 & E_{t,k} & 0\\ 0 & 0 & 0\end{bmatrix}\begin{bmatrix}\epsilon_{nn}\\ \epsilon_{tt}\\ \gamma_{nt}\end{bmatrix}_k \tag{9}$$

The strain vector now includes index k, as the axes of orthotropy n_k and t_k differ per fraction. Once the tangential stress $\sigma_{tt,k}$ reaches the compressive or tensile strength of the fraction, a secondary crack is allowed to form. After the formation of this second crack, the complete capacity of the considered fraction is lost. The stresses on element level, which is represented by Fig. 2(A), are found by superposition of the stresses in the individual fractions. In this way, the element stress vector $\boldsymbol{\sigma}$ is obtained by

$$\boldsymbol{\sigma}(\boldsymbol{\epsilon}) = \frac{1}{t}\sum_{k=1}^{N}\boldsymbol{\sigma_k}(\boldsymbol{\epsilon})\Delta t_k \quad \text{with} \quad t = \sum_{k=1}^{N}\Delta t_k \tag{10}$$

Likewise, the element stiffness matrix is also found by superposition over the parallel fractions. In summary, once a fraction cracks, it starts behaving orthotropic rather than isotropic and the crack direction of that fraction is fixed. The transition of a fraction from isotropic to orthotropic behaviour influences the stresses and strains on element level: the summation of cracks is changed due to the formation of another crack and eventually, the direction of the overall conceived crack on element level might change, hence mimicking a rotating crack.

4.1.2. Defining the material properties of each fraction

In sequentially linear analysis, the constitutive continuum law is discretised to a saw-tooth or step-wise secant material law (for example Fig. 1). The Young's modulus and tensile strength of each elastic-perfectly brittle fraction can be chosen such that the superposition of fractions results in a specific saw-tooth curve, under the assumption of monotonically increasing proportional loading.

For instance, if we envision a homogeneous uniaxial tension case, each individual elastic brittle fraction is characterised by its thickness, Young's modulus and tensile strength in order to represent the overall saw-tooth softening law. The remaining stress at a specific moment is the superposition of the stresses of the uncracked fractions. Starting from the last fraction to crack (with the largest ultimate strain), the fraction properties can be determined in a backwards recursive manner, using the elements stress–strain saw-tooth law as required for regular SLA. As the fraction properties are determined starting from the last layer ($i = N$), a new index

$$k = N - i + 1 \tag{11}$$

is introduced, which takes value 1 for $i = N$ and N for $i = 1$. In this way, the fraction with the largest strain $\epsilon_{t/c,i}$ has index $k = 1$.

For the determination of the fraction properties, either the thickness Δt_k^L or stiffness E_k^L should be predefined since the membrane stiffness of a fraction is proportional to $\Delta t_k^L E_k^L$. In the following, it is assumed that all fractions have the same thickness $\Delta t_k^L = t/N$. By doing so, the contribution of the stress of the considered fraction to the total element behaviour is σ_k^L/N. The stress is summed over the total element thickness t. The same holds for the fraction stiffness.

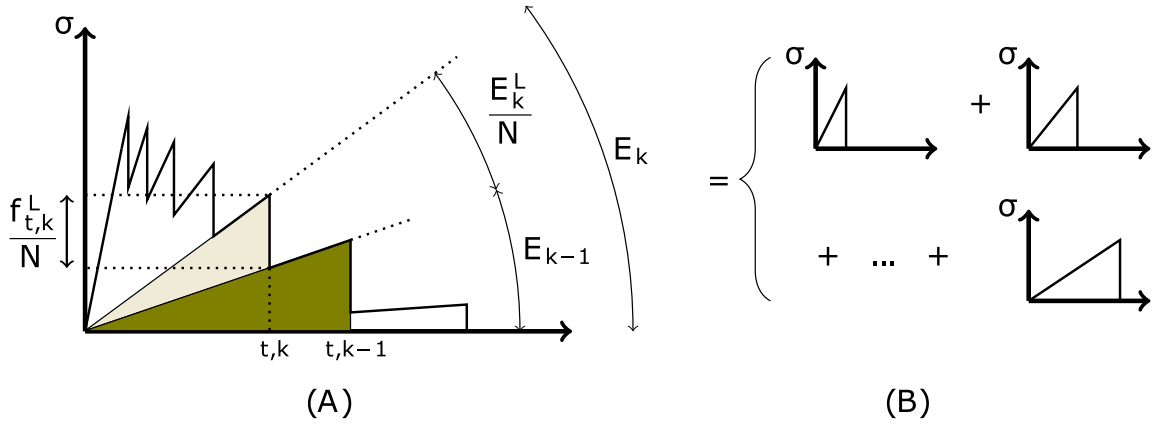

Fig. 3. The task of determining the Young's moduli and tensile strengths of individual elastic-brittle fractions (B) such that the superposition represents the overall ripple band saw-tooth law (A).

Table 1
Example of transition from the saw-tooth curve (SLA) to elastic-brittle fraction properties corresponding to the fraction model (FM), based on ripple band parameter $p = 0,25$.

SLA Ripple band			FM ripple band		
i	E_k (N/mm^2)	$f_{t,k}$ (N/mm^2)	k	E_k^L (N/mm^2)	$f_{t,k}^L$ (N/mm^2)
1	10000	1.17	4	17143	2.00
2	5714	0.93	3	12245	2.00
3	2653	0.61	2	8746	2.00
4	466	0.15	1	1866	0.60

The given collection of damaged stiffnesses E_k from the saw-tooth curve are used to determine the fraction stiffnesses E_k^L according to Fig. 3. As both damaged stiffnesses E_k and E_{k-1} are known, and the difference between the both of them is the stiffness contribution of fraction k with respect to the complete element thickness E_k^L/N, the following equality can be set up

$$E_k = \frac{E_k^L}{N} + E_{k-1} \tag{12}$$

The physical meaning of Eq. (12) is visualised in Fig. 3; both the left hand side and right hand side should give the same total stiffness. From Eq. (12) E_k^L is solved, giving

$$E_k^L = N(E_k - E_{k-1}) \tag{13}$$

With the aid of Eq. (13), the stiffness of a specific fraction k can be derived from the damaged stiffnesses following from the saw-tooth law. In Fig. 3, the two filled areas represent two separate fractions. The tensile strength $f_{t,k}^L$ of fraction k is obtained by

$$\frac{f_{t,k}^L}{N} = \frac{E_k^L}{N}\epsilon_{t,k} \quad \text{hence} \quad f_{t,k}^L = E_k^L\,\epsilon_{t,k} \tag{14}$$

Invoking Eqs. (13) and (14), all properties of a fraction k have been determined: thickness Δt_k^L, stiffness E_k^L and tensile strength $f_{t,k}^L$. The fraction model, in principle, also allows for individual fractions to have different thicknesses but the young's moduli may have to be adapted accordingly.

The transition from an arbitrary saw-tooth curve to the fraction model is shown by the following example. A linear tension softening constitutive law is considered with tensile strength $f_t = 1\,\text{N/mm}^2$, stiffness $E_0 = 10{,}000\,\text{N/mm}^2$, mode I fracture energy $G_f = 0.15 \cdot 10^{-3}\,\text{N/mm}$ and crack band width $h = 1$ mm. Using the ripple band formulations from [14] with $p = 0.25$, a saw-tooth curve consisting of 4 saw-teeth is obtained. With the aid of Eqs. (13) and (14), whilst assuming the same thickness for all the fractions, stiffness E_k^L and tensile strength $f_{t,k}^L$ are retrieved and listed in Table 1.

4.1.3. Elastic-brittle fraction model within the context of SLA

The elastic-brittle fraction model fits well within the framework of regular sequentially linear analysis. Fig. 4 presents the flowchart of the model, where the additional step in the algorithm compared to regular SLA is highlighted. First, the saw-tooth law(s) is (are) generated in step (1) based on for example the Ripple band approach and a specific continuum law. Based on the saw-tooth curve, elastic-perfectly brittle fractions are generated in step (2) such that on element level the same constitutive material behaviour is found. The output of this step are strength, stiffness and thickness properties for each of the fractions. Step (2) is an extra step that is required for the fraction model compared to SLA. Next, a linear analysis is performed in step (3), the most critical

integration point is traced in step (4) and the analysis results are scaled with the critical load multiplier in step (5). The SLA procedure is stopped in step (6) once a specific user-defined damage state is reached (e.g. a maximum number of damage increments). If the stop criteria is not fulfilled, a brittle damage increment is applied in step (7) and the stiffness perpendicular to the formed crack is set to 0.

Within the flowchart of Fig. 4, steps (1) and (2) take place at an element level, steps (3) till (6) occur at a structural level and step (7) is performed on fraction level. On a structural level, a damage increment is applied to only 1 critical integration point at a time. Therefore, the crack direction can only rotate at the considered critical element and the other elements are forced to follow a fixed cracking approach. When interpreting the fraction model as merely rotational cracking for the critical element, similarities with the approaches of Slobbe [33], taking a rotating crack as an event, and Vorel and Boshoff [27], updating the principal directions of the critical integration point after each stress redistribution, become evident. Instead of updating the crack rotation on element level for a critical element like Slobbe, a damage increment on fraction level is performed, representing a crack rotation on the critical element level. While the approach of Slobbe considers damage increments and crack rotations separately, the fraction model simulates crack rotations by applying damage increments, marking a clear difference between the two approaches. Instead of requiring an incremental iterative stress redistribution to redistribute stresses after a damage increment like Vorel and Boshoff, the fraction model is a purely sequentially linear approach, where redistribution takes place in the subsequent steps. On top of that, crack directions are fixed upon initiation on fraction level, where Vorel and Boshoff update the crack directions on element level during the remainder of the analysis for the critical integration points.

The model also shows similarities with the approach of Cook et al. [31]. In the fraction model, fractions are predefined with potentially each their own crack direction. Following the same line of thinking, the model of Cook et al. simulates a rotating crack as a multi-directional crack with predefined cracking planes, having each their own predefined crack direction. The most critical plane (instead of fraction) is sought for and a damage increment is performed. However, while the model of Cook et al. requires a large amount of predefined cracking planes on element level, each fraction of the fraction model is allowed to crack in any direction, depending on the principal stress direction, and therefore, a wide spectrum of cracks can be simulated without the need to predefine a large amount of cracking planes apriori. Furthermore, similarities exist with the microplane model [35] in the sense that damage can be obtained on planes of various orientations called microplanes.

The constitutive framework in use in SLA is the total strain based smeared cracking model. It has been established in literature that these models based on the crack band approach reproduce the size effect observed in brittle failures adequately using the softening laws. However, they have limitations with respect to mesh refinement, shear locking on zig-zag crack bands, and mesh directional bias [36]; all of which are associated with the FE mesh. These features are therefore expected to a certain extent in the fraction model as well. But investigations on this topic are out of the scope of this study and are reserved for future studies.

4.2. 3-dimensional framework

SLA applied to 3D solid elements under proportional loading had been developed earlier [37]. A further elaboration to non-proportional loading in 3D was recently published [25]. Furthermore, [24] incorporated shell elements in the framework of SLA. In fact, the application of SLA to shell or solid elements is governed by the same principles as the 2-dimensional framework: upon damage initiation, the axes of orthotropy are fixed, along which the stresses are monitored during the remainder of the analysis, and once the saw-tooth strength is reached, damage increments are performed along that specific axis according to the specified saw-tooth law. In 2D, damage increments are allowed in n,t-directions and in 3D, damage can take place in n,s,t-directions. The definition of the uniaxial saw-tooth laws does not change.

In 3D, in line with the 2D elastic-brittle fraction model, the total volume of the element (or volume corresponding to an integration point) is split in elastic perfectly brittle overlay elements, each having their own stiffness, strength and fixed crack direction. In this way, the 3D model utilises a fixed cracking model per fraction and mimicks a rotating crack on element level. For 2D, it was arbitrarily assumed that all fractions have the same thickness t_0/N. In 3D, all fraction elements are assumed to have a volume that is equal to the total elements volume. In Fig. 5, solid fraction elements (A), (B) and (C) all have the same volume as total element (D). Each of the fraction elements has its own fixed axes of orthotropy.

Upon crack initiation in a specific fraction, a transition is made from the undamaged isotropic stiffness matrix to the damaged 3D orthotropic stiffness matrix and a brittle damage increment is performed in the local n-direction of that fraction. Hence, the stress–strain relation reduces to

$$\begin{bmatrix}\sigma_{nn}\\ \sigma_{ss}\\ \sigma_{tt}\\ \sigma_{ns}\\ \sigma_{st}\\ \sigma_{tn}\end{bmatrix} = \frac{1}{1-\nu_{ts}\nu_{st}}\begin{bmatrix}0 & 0 & 0 & 0 & 0 & 0\\ 0 & E_s & \nu_{st}E_s & 0 & 0 & 0\\ 0 & \nu_{ts}E_t & E_t & 0 & 0 & 0\\ 0 & 0 & 0 & 0 & 0 & 0\\ 0 & 0 & 0 & 0 & \left(1-\nu_{ts}\nu_{st}\right)G_{st} & 0\\ 0 & 0 & 0 & 0 & 0 & 0\end{bmatrix}\begin{bmatrix}\epsilon_{nn}\\ \epsilon_{ss}\\ \epsilon_{tt}\\ \gamma_{ns}\\ \gamma_{st}\\ \gamma_{tn}\end{bmatrix} \tag{15}$$

In the s,t-plane, secondary and tertiary cracks can develop in the s and t-directions respectively. Once the tensile strength of a fraction is reached in either the s or t-direction, a brittle damage increment is performed in the critical direction. For example,

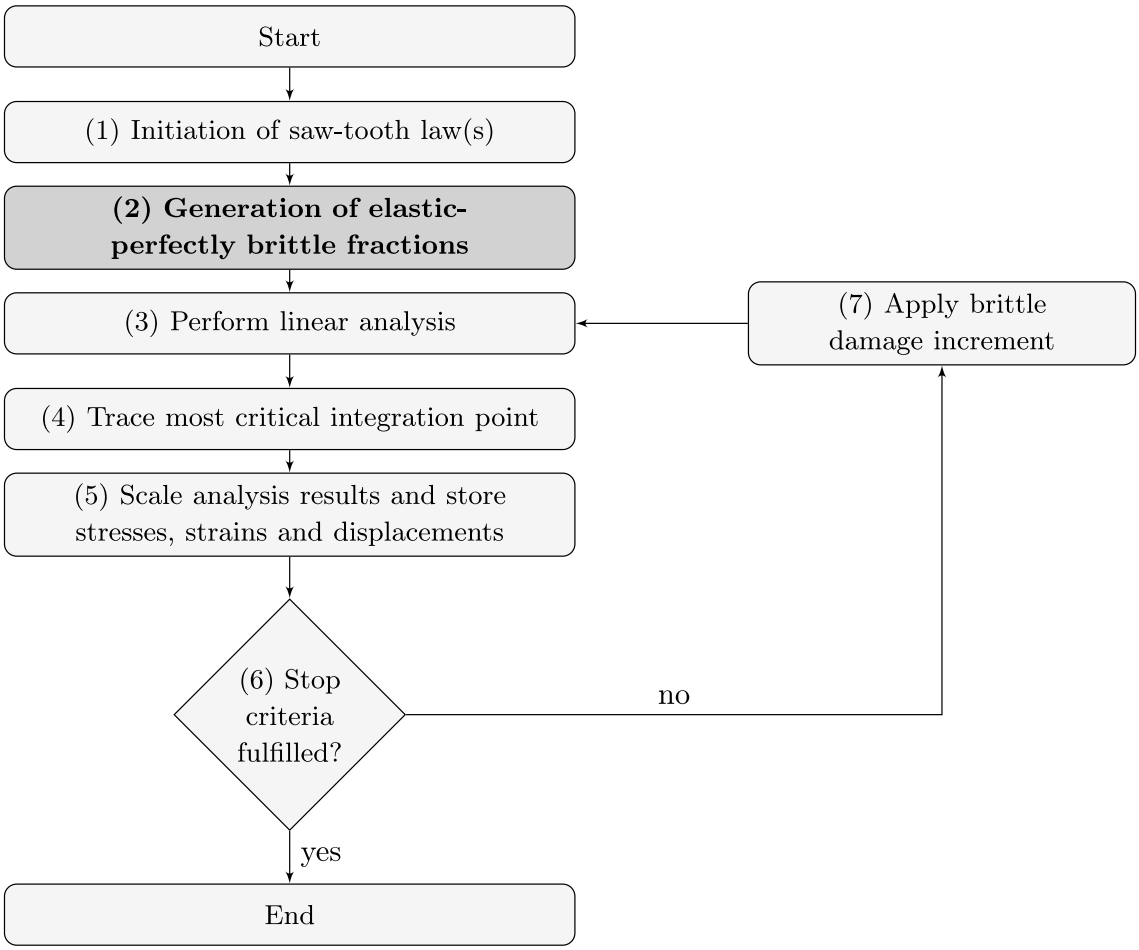

Fig. 4. Conceptual flowchart of the elastic-brittle fraction model within the framework of SLA. Compared to SLA, an additional step is required (step 2, highlighted).

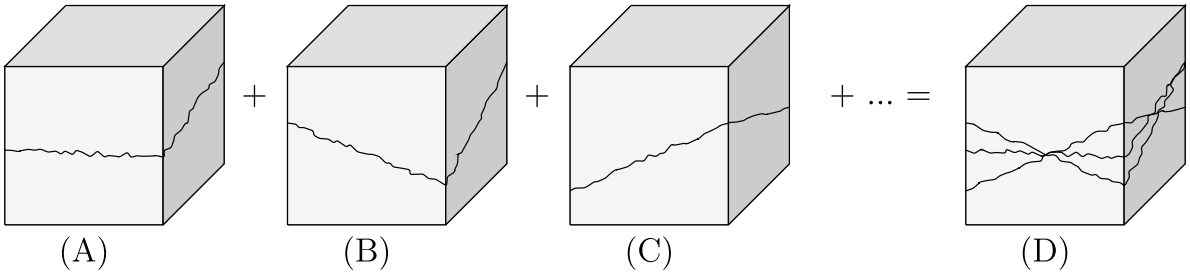

Fig. 5. Superposition of fraction elements (A), (B) and (C) with fixed cracking plane, leading to total element (D) with a multi-directional crack.

when the tensile strength is reached in the s-direction, $E_s = 0$ and therefore $\nu_{ns} = \nu_{ts} = G_{st} = 0$, such that

$$\begin{bmatrix} \sigma_{nn} \\ \sigma_{ss} \\ \sigma_{tt} \\ \sigma_{ns} \\ \sigma_{st} \\ \sigma_{tn} \end{bmatrix} = \begin{bmatrix} 0 & 0 & 0 & 0 & 0 & 0 \\ 0 & 0 & 0 & 0 & 0 & 0 \\ 0 & 0 & E_t & 0 & 0 & 0 \\ 0 & 0 & 0 & 0 & 0 & 0 \\ 0 & 0 & 0 & 0 & 0 & 0 \\ 0 & 0 & 0 & 0 & 0 & 0 \end{bmatrix} \begin{bmatrix} \epsilon_{nn} \\ \epsilon_{ss} \\ \epsilon_{tt} \\ \gamma_{ns} \\ \gamma_{st} \\ \gamma_{tn} \end{bmatrix} \tag{16}$$

which is completely in line with the 2D fraction model after a brittle damage increment in the primary crack direction (see Eq. (9)). Once the tensile strength is reached in the tertiary crack direction as well, the complete load carrying capacity of the fraction vanishes.

The transition from SLA to the elastic-brittle fraction model requires some minor changes compared to the 2-dimensional framework. In the 2D model, it is assumed that all fractions have the same thickness t_0/N. For the 3D model, all fraction elements have the same volume and thus the same dimensions as the total element. To that end, the derivation of Eqs. (13) and (14) slightly changes: the contribution of a single fraction does not have to be scaled to the total element volume, since the fraction already has the same dimensions as the total element. Therefore, the stiffness contribution of a single fraction to the total element behaviour changes from E_k^L/N to E_k^L and the stress contribution changes accordingly. Hence, the fraction element properties in 3D are determined by

$$E_k^L = E_k - E_{k-1} \tag{17}$$

and

$$f_{t,k}^L = E_k^L \, \epsilon_{t,k} \tag{18}$$

Invoking Eqs. (17) and (18), all properties of the 3D fraction elements are determined: volume V_0, stiffness E_k^L and tensile strength $f_{t,k}^L$. Apart from the aforementioned differences, the algorithm as schematised in Fig. 4 remains the same for the 3D-framework.

5. Validation studies

The presented elastic-brittle fraction model is validated in this section firstly at the single element level using a tension-shear problem. Thereafter, three validation studies of structural case studies are presented: a notched beam and a shear notched beam case study, both testing in three-point bending; and a concrete gravity dam subject to lateral loading. Finally, the 3D elastic brittle fraction model is validated using an inclined notched beam case tested in three-point bending. Analyses using SLA with the fixed crack model are hereon referred to as *regular* SLA or SLA as such.

5.1. Tension-shear problem

It is expected that for situations where the principal stress directions do not change, the presented elastic-brittle fraction model will give exactly the same results as SLA. Therefore, a tension-shear model example is used here to study differences. This section entails the analysis of a tension-shear problem proposed by William et al. [38], which is visualised in Fig. 6. A single four-node quadrilateral isoparametric plane stress element with thickness $t = 1$ mm and 1 integration point is considered, with material parameters as listed in Table 2 and a crack band $h = 1$ mm. The continuum law is described by a linear tension softening relation with ultimate strain $\epsilon_u = 3.00 \cdot 10^{-3}$. Two loading stages are prescribed:

- First, the element is loaded by tensile straining $\Delta\epsilon_{xx}$ combined with vertical compressive straining $\Delta\epsilon_{yy} = -\nu_0 \, \Delta\epsilon_{xx}$ to simulate Poisson's effects in the y-direction, and a tensile crack perpendicular to the tensile load is formed.
- Second, at the onset of cracking, the loading is changed to a combined biaxial tension and shear loading according to: $\Delta\epsilon_{xx} : \Delta\epsilon_{yy} : \Delta\gamma_{xy} = 0.5 : 0.75 : 1$, resulting in a rotating crack, as shown by Fig. 6. The loading of stage (A) remains on the element during stage (B), and hence, non-proportional loading is obtained.

The displacements of the bottom left node are fixed to zero and the displacements of the other three nodes are prescribed such that the element follows the applied strain fields for both loading stages. A very small ripple band parameter $p = 0.01$ is applied, leading to $N = 83$ fractions, in order to approximate a continuous solution that allows for a one-to-one comparison. Three types of analyses are performed: (1) NLFEA based on a rotating crack model with damage based reduction of the Poisson's ratio, (2) Regular SLA with variable shear retention according to Eq. (5) and $p = 0.01$ and (3) the fraction model with elastic perfectly brittle fractions and $p = 0.01$. Fig. 6 entails a graphical representation of the cracking process using the fraction model. After damage initiation in the first stage, the second load leads to a rotating crack in steps (B)–(E) due to the non-proportional loading. At step (E), for $\gamma_{xy} = 2.08 \cdot 10^{-3}$, a primary crack is formed in all fractions and the ultimate strain is reached normal to the crack. From this point on, secondary cracks form as the remaining uncracked part of the element is still capable of carrying some load. At any moment, the primary crack angle of the critical fraction is equal to the principal strain direction and therefore, this specific fraction has the same crack angle as a rotating crack in NLFEA.

The shear response $\sigma_{xy} - \gamma_{xy}$ of all three analyses is plotted in Fig. 7. When comparing regular SLA with NLFEA results, clear differences are observed in the shear behaviour as regular SLA is prone to significant stress locking effects. After damage initiation, the crack angle of SLA is fixed vertically and a rotation of principal stresses is not followed. Stresses are only monitored within the fixed cracking plane, while stresses exceeding the capacity might take place in a different direction and therefore, spurious stresses are obtained. These also depend on the shear retention along the fixed crack, i.e. if a shear retention function $\beta = 0$ were to be used there would be no shear stresses across the crack plane. Since these spurious stresses exceed the capacity of the material, they are often referred to as stress locking or stiffening effects. These stiffening effects are clearly observed in the shear stress response of SLA. Contrarily, the fraction model entails much less pronounced stress locking effects and approximates the rotating crack NLFEA better. No significant shear stress overshoot is obtained and a similar trend as the rotating crack model is followed. However, it

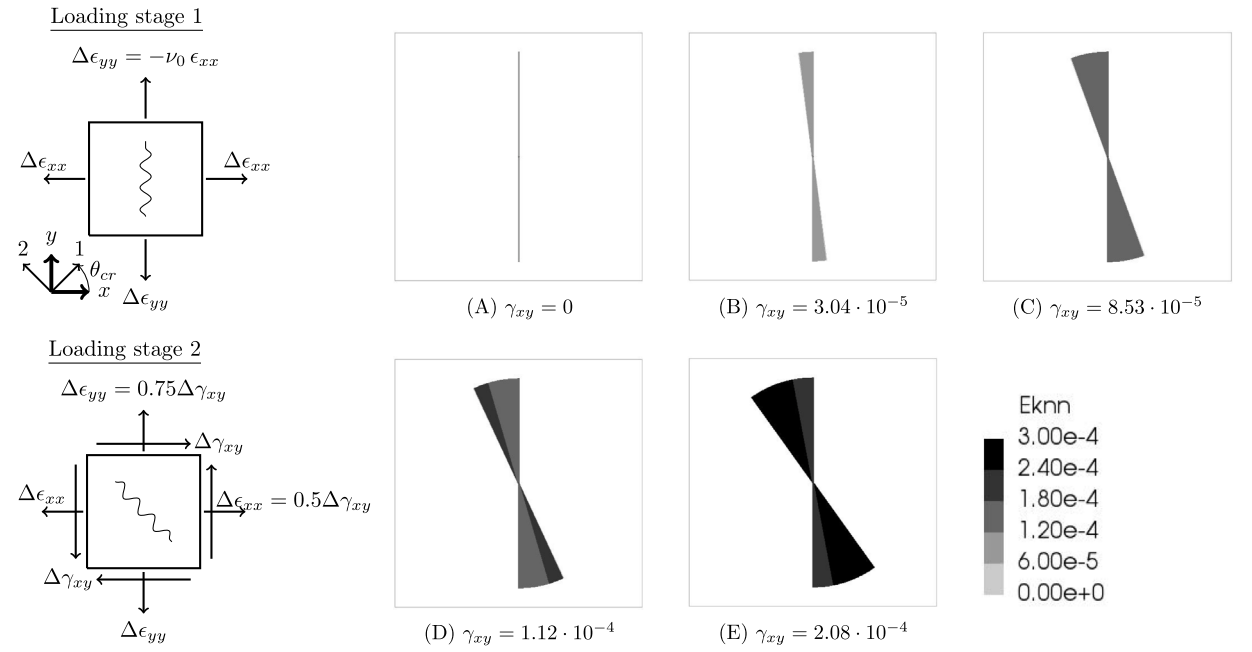

Fig. 6. Loading stages of the tension-shear problem (1) tensile loading up until first damage and (2) tension-shear loading (left); and (A)–(E) crack development for specific γ_{xy} in the fraction model, mimicking a rotating crack with *Eknn* the normal strain in a crack ($\epsilon_u = 3.00 \cdot 10^{-4}$) (right).

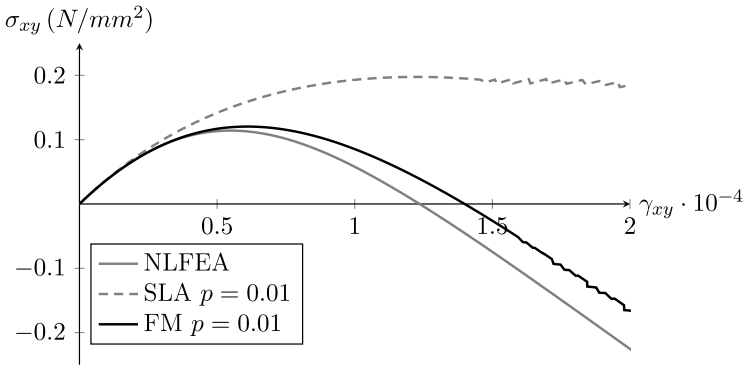

Fig. 7. Tension-shear problem: shear stress σ_{xy} versus shear strain γ_{xy} for NLFEA, SLA and the elastic-brittle fraction model (FM).

is noted that some differences are still found due to the influence of earlier cracked fractions with crack directions deviating from the current principal stress direction. Furthermore, on the structural level, interaction between adjacent elements takes place and therefore, deviations and error propagation do not solely depend on the single elements crack angles, but on the structural behaviour as a total, and this is investigated in the upcoming case studies.

5.2. Bending notched beam

The first structural case considered is a notched beam tested in three point bending, which is widely used as a benchmark test [18,21] to study the performance of finite element models in regard to cracking and localisation behaviour in quasi-brittle materials. For this study, the geometry as shown by Fig. 8 and experimental results are taken from the study performed by Zhao et al. [39,40]. Beam specimen SG2-B1 of the mentioned experimental program is examined in this study, the thickness of which is t = 120 mm. Material properties are as presented in Table 2, retrieved from Van de Graaf [18], who slightly adapted the material properties as presented in [40] to better fit the experimental data. A mode–I tensile fracture mode is observed above the notch as a result of tensile bending stresses. The size of the notch is taken to be equal to the size of a single finite element.

For both regular SLA and the fraction model, analysis is performed with 8-node quadrilateral isoparametric plane stress elements of size 10 mm with 2 × 2 Gaussian integration. The linear tension softening law is used. A ripple band parameter $p = 0.1$ is applied, leading to $N = 25$ fractions with crack bandwidth $h = 5$ mm. The load–displacement graphs for both regular SLA and the fraction

Table 2
Material parameters for the case studies.

Quantity	Case study				
	Tension-shear problem	Notched beam	Shear Notched beam	Reduced scale gravity dam	3D Inclined Notched beam
Tensile Strength f_t (N/mm^2)	1.0	3.78	2.8	3.6	3.78
Initial Stiffness E_0 (N/mm^2)	10000	16000	24800	35700	16000
Poisson's ratio v_0	0.15	0.15	0.18	0.1	0.15
Mode-I fracture energy G_1^f (N/mm)	$0.15 \cdot 10^{-3}$	0.30	0.15	0.184	0.30
Tension softening law	Linear	Linear	Hordijk	Linear	Hordijk
Ripple band parameter p	0.01	0.1	0.115	0.12 , 0.13	0.2
Crack bandwidth h (mm)	1	5	8	30 , 21.21	6

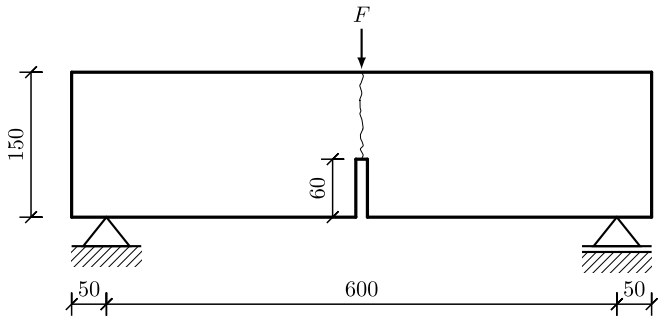

Fig. 8. Geometry of the notched beam case with all dimensions in mm.

model are presented in Fig. 9 (left). Furthermore, the corresponding crack patterns for regular SLA and the fraction model based on linear tension softening for a mid-span displacement of 1.0 mm are depicted in Fig. 9 (right).

Spurious stresses obtained in FE simulations with smeared cracking models are primarily due to the stress-locking effects observed in the single element tension-shear problem in the previous section, which appear to be significantly reduced by the fraction model. However, when large localised deformations take place in a specific element, surrounding elements inherently are also subject to deformations to some extent. This induces spurious stresses in the neighbouring elements resulting in their cracking, due to the inability to follow the discontinuous nature of the displacement field across the crack in the smeared cracking concept (contrary to discrete cracking) [2,32].

In Fig. 9 (right(A)–(B)), black lines represent fully developed cracks and grey lines depict cracks that are initiated but still in development. Both regular SLA and the fraction model reveal the development of spurious stresses due to the inability to follow the discontinuous displacement field across the crack. However, while an increasingly asymmetric state is observed for regular SLA, the fraction model is able to correct its crack direction by sequential cracking of the different fractions with each of their own crack directions. Hence, spurious stresses and cracks due to incorrect crack directions for the fraction model are limited and a slightly narrower localisation band is observed in Fig. 9 (right(B)). In the same figure, significant crack rotations are observed at the top of the crack, while Fig. 9 (right(A)) reveals an incorrect crack direction for SLA. It is understood that the unique advantage of SLA to follow asymmetric failure modes and overcome bifurcations, as mentioned by Rots et al. [41], comes with the disadvantage of potentially enforcing locally asymmetric failure modes for inherently symmetric problems. The fraction model is still able to overcome bifurcations by following asymmetric failure modes, but is meanwhile able to correct itself when the asymmetric failure mode is undesired (e.g. for symmetric cases). Due to the aforementioned reasons, differences between the load–deflection curves of regular SLA and the fraction model are found in Fig. 9 (left): i.e. the reduction of spurious stresses results in less energy dissipation, and therefore a less stiff response of the fraction model compared to regular SLA, especially in the post-peak regime.

Lastly, the crack localises within half of the element, which is included in the applied crack band. According to Slobbe [42], when using higher order elements, stress fields become highly disturbed due to strain localisation within an element and an increase of spurious stresses is expected. The crack plots support this statement: a wide band of spurious cracks is obtained. In a paper by Slobbe et al. [21] on a delayed crack path fixation approach, so-called U-turns of the crack paths in the notched beam were observed for quadratic (8-node) elements, manifesting themselves in sudden and unrealistic sharp changes of crack paths, as shown by Fig. 10. The crack bends sideways and then turns around. Similar cracking paths are observed in this study in Fig. 9 (right-A) (crack strains averaged over the element and at their respective centroids), as the crack also bends sideways and some near horizontal cracks are found at the top of the crack. Contrarily, the fraction model seems to resolve the appearance of a U-turn: the crack path stays at the center-line column of elements instead of diverging to a different column of elements, although significant crack rotation is required in the top elements for this purpose. The reduction of spurious stresses indicates that the underlying reason for the occurrence of U-turns must be sought for in the fixed crack assumption that is the basis for regular SLA. The latter statement is supported by the load–deflections curve in Fig. 9 (left): very pronounced differences are found in the post-peak responses of regular SLA and the

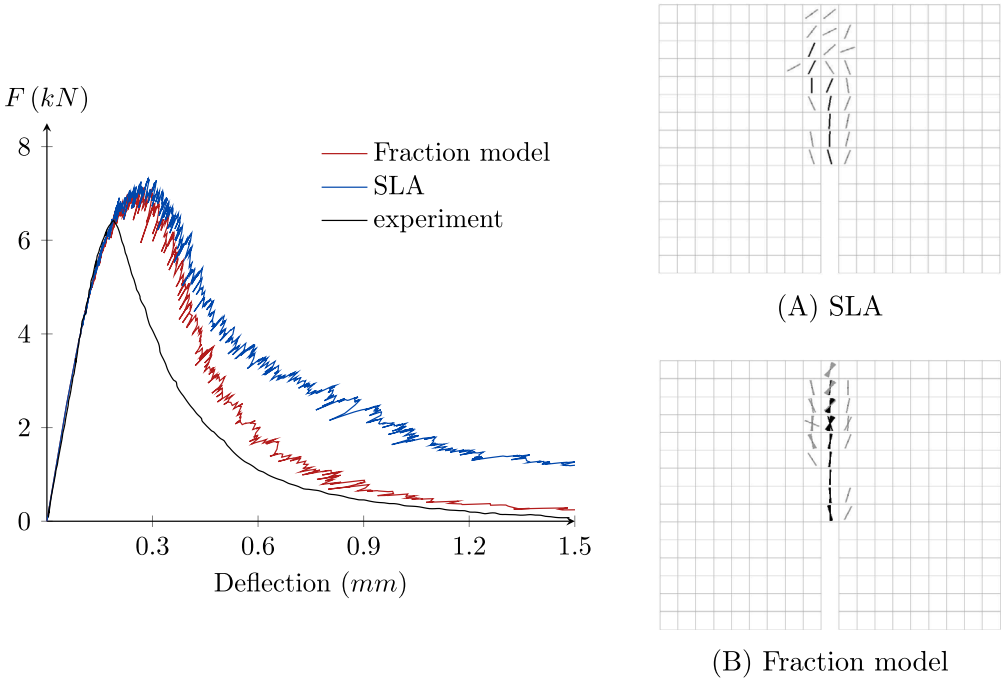

Fig. 9. Load versus displacement at mid-span for the notched beam case, based on linear tension softening (left), and the crack strain plots averaged over the element for regular SLA (A) and that of the fraction model (B) of the notched beam for a mid-span deflection of 1.0 mm.

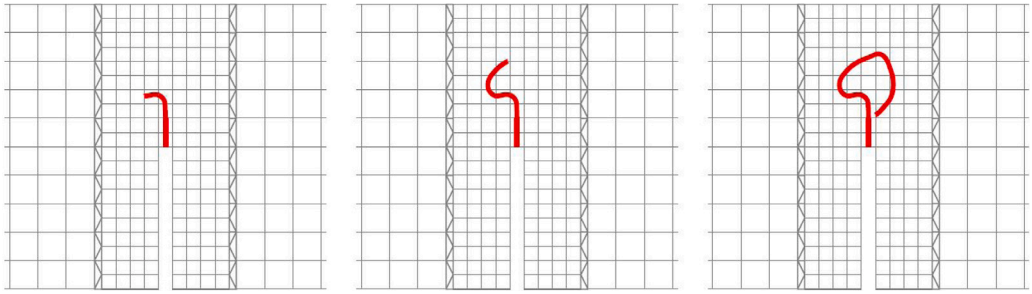

Fig. 10. The development of a so-called U-turn for quadratic (8-node) elements, where the crack path is marked in red and taken from Slobbe et al. [21].

fraction model as a result of the restrained U-turn and reduction of spurious stress development. Much stiffer behaviour is obtained when using regular SLA, which is clearly not in line with the experimental results, while the fraction model shows a rather flexible reduction to zero load bearing capacity.

5.3. Shear notched beam

The second case that is considered is the shear notched beam, also known as the four-point shear test. The curved crack pattern, that is found right above the notch and propagates towards the load F, has been used by many authors [2,42–47] to study the performance of a wide variety of smeared and discrete crack models in mixed-mode crack propagation. In this study, the geometry and the experimental results of Series C of the research program performed by Arrea [48] are used. The beam specimens have a thickness t = 156 mm and a geometry as shown by Fig. 11. For series C, three beams were tested, of which only two were considered to be valid. For that reason, some significant scatter is observed in the results as well as in the material properties of the specimens. In the experimental program, only the compressive strength, stiffness and Poisson's ratio were measured, and information on the tensile strength and fracture energy is missing. In this study, the tensile strength f_t, stiffness E_0 and Poisson's ratio ν_0 are taken from Rots [2], which are frequently used by other references as well. Regarding the fracture energy, values between 0.075 and 0.2 N/mm are found in the given references and G_1^f = 0.15 N/mm is applied for this study to be somewhere in the middle. Table 2 lists the applied material properties.

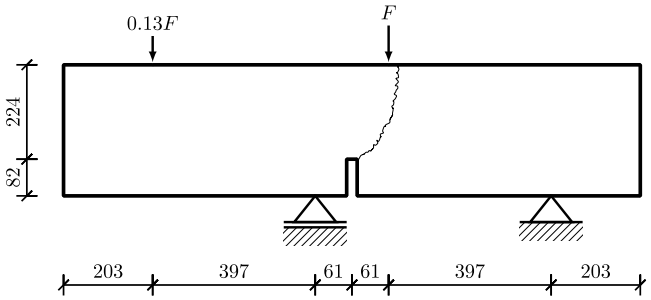

Fig. 11. Geometry of the Shear notched beam case with all dimensions in mm.

The shear notched beam case results in a combined mode I and mode II fracture. The case is mainly governed by mode I tensile crack development above the notch, and the generation of mode II shear cracks is rather limited. According to Rots and De Borst [49], the shear notched beam releases the mode I fracture energy much quicker than the mode II fracture energy. Although an analysis considering only mode I fracture is therefore justified for the purpose of this study, it is noted that in reality pure mode I fracture is not obtained and one should actually consider mode II shear fracture patterns as well for a complete description of this case.

The specimen is modelled using 8-node quadrilateral isoparametric plane stress elements of size 8 mm with 2×2 Gaussian integration. Around the notch, nonlinear material behaviour following Hordijk tension softening [50] is assumed. A ripple band parameter $p = 0.115$ is applied, leading to $N = 19$ fractions with crack bandwidth $h = 8$ mm. Nonlinear material behaviour is only allocated to the relevant part of the beam to reduce computational efforts. Furthermore, the outer 203 mm of the beam in Fig. 11 is not modelled for the same reasons. Around the notch, smaller elements are used compared to the rest of the beam, 8 mm and 16 mm respectively, to have a sufficient level of detail. The loading and support close to the notch are both modelled with an extra row of elements, to prevent influence of stress concentrations due to the applied load. Crack bandwidth is chosen according to an assumed zig-zag propagation pattern [2]. The width of the notch is taken equal to the size of a single element.

During the analyses, the crack mouth sliding displacement (CMSD) is monitored, defined as the difference in vertical displacement between the two sides of the notch, considered at the height of the supports. The CMSD-load curves for all three cases and the experimental results [48] are shown by Fig. 12 (top-left). The corresponding crack patterns for a CMSD of 0.20 mm for both regular SLA and the fraction model are depicted by Fig. 12 (right(A)–(B)), and a comparison of the crack widths is made in Fig. 12 (bottom-left) wherein the experimental crack band as reported by Cendon et al. [44] is used. The coordinate center is defined at the right bottom corner of the notch.

The crack pattern that is found by the fraction model exhibits a smaller localisation band compared to regular SLA as observed in Fig. 12 (bottom-left), indicating a reduction of spurious cracks and stresses. Crack rotations, as has been previously stated, influences the structural response in two ways: on single element level and on structural level. Firstly, a more up-to-date crack angle is obtained and less spurious stresses are observed within the element, as the stresses are monitored in a plane that is more in line with the critical plane and the occurrence of stresses exceeding the elements capacity is reduced (which is not the case for the fixed crack model). Secondly, over stiff behaviour on single element level induces the generation of spurious stresses in neighbouring elements as well in regular SLA. Due to stiffening, larger stresses are accepted for the cracked element, causing surrounding elements to crack while the considered element should crack, generating spurious cracks. Therefore, the observed smaller localisation band on structural level for the fraction model is due to the more flexible behaviour on the element level as compared to regular SLA. Fig. 12 (right(A)–(B)) further substantiates the smaller localisation band of the fraction model. Quite substantial deviations are found compared to the experimental crack patterns, especially in the vertical branch of the crack, which is probably the result of the mesh following tendency, better known as mesh directional bias. When comparing the CMSD-load curves of both methods, more flexible behaviour is obtained using the fraction model in the post-peak regime, supporting previous findings. The results are in good agreement with experimental results as well. According to Rots [2], in case of fracture, prediction of genuine separation and softening down to zero load is desired, and it was observed that smeared crack approaches were not able to fulfil these requirements. However, in this study, both regular SLA and the fraction model tend to predict an ultimate softening down to zero, although the fraction model seems to reach this state quicker. In this case study, at a CMSD of 0.20 mm, the fraction model finds a load of 17.7 kN, while regular SLA results in 26.5 kN, being 49.7% higher compared to the fraction model. In conclusion, the elastic-brittle fraction model again results in slightly sharper localisation bands, less stress locking, and a more flexible post peak response in line with the findings of the studies of the previous sections.

5.4. Reduced scale gravity dam

Over the years, the experiments performed by Carpinteri et al. [51]; wherein two scaled down 1:40 models of a concrete gravity dam, with geometry as shown in Fig. 13, were subjected to lateral loading representing a hydro-static pressure along the upstream side of the dam; have been simulated by many authors [43,47,52,53]. Initially, the goal of the experimental program was to include a certain multiplier of the self-weight (to account for scale-effects) as well in the loading. However, a test including simulation

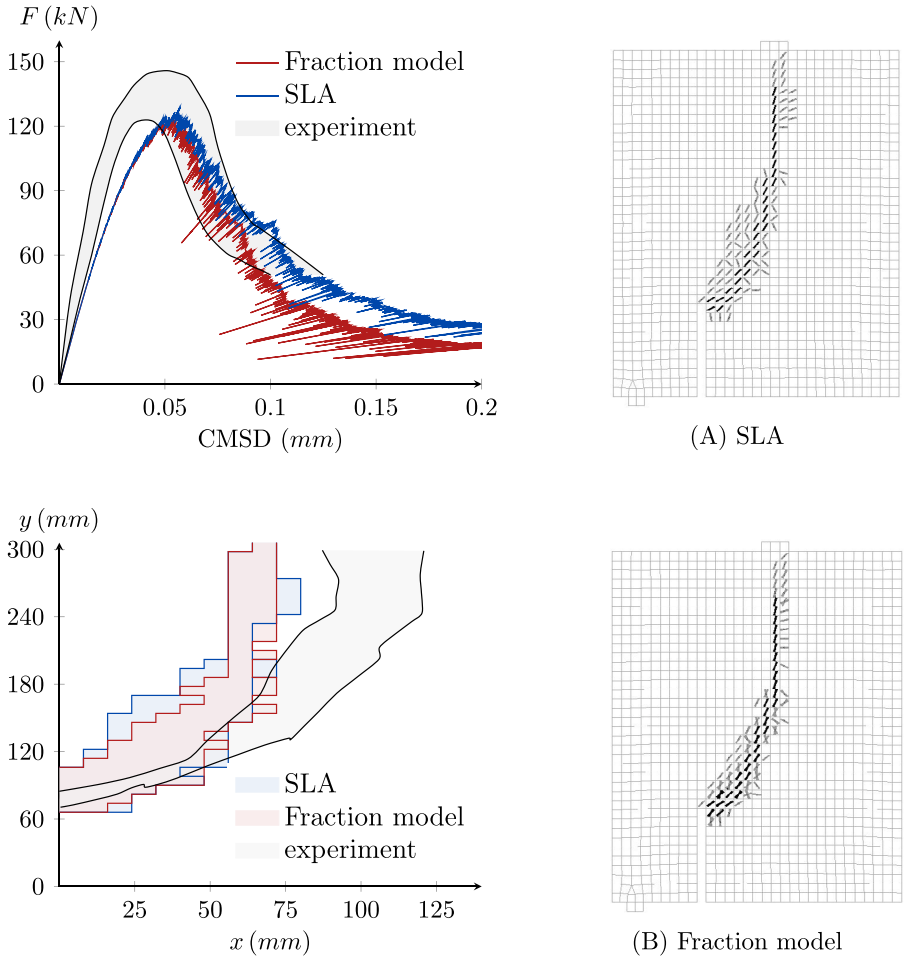

Fig. 12. Load on the shear notched beam versus crack mouth sliding displacement (CMSD) for the case considered using SLA and fraction models compared against the experiment (top-left); comparison of crack paths of the SLA and fraction models with experimental bounds for a CMSD of 0.20 mm (bottom-left); and crack strain plots for regular SLA (A) and the fraction model (B) for a CMSD of 0.20 mm.

of self-weight had to be stopped prematurely. Hence, the scaled concrete dam was loaded by a proportional load. In this study, 'test 3' with a notch/depth ratio of 0.2 is simulated. The specimen has a thickness of 30 cm and material properties are taken from Carpinteri et al. [51] and listed in Table 2. During the experiment, a curved crack path propagating towards the downstream bottom side of the dam was observed.

In line with the aforementioned references of numerical simulation of the case study, the hydro-static pressure at the dam is simulated with the aid of 4 equivalent lateral point loads, such that F (see Fig. 13) equals the integrated hydro-static pressure over the height of the dam. Lateral and vertical displacements are restrained at the bottom of the specimen. In order to reduce computational efforts, nonlinear material behaviour is only assigned to the bottom part of the meshes. Two variations are made: First, a mesh with 8-node quadrilateral isoparametric plane stress elements of size 30 mm with 2×2 Gaussian integration scheme. A ripple band parameter $p = 0.12$ is applied, leading to $N = 14$ fractions with crack bandwidth $h = 30$ mm. Second, a mesh with 6-node triangular isoparametric plane stress elements of size 30 mm with a 3 point Gaussian integration scheme. A ripple band parameter $p = 0.13$ is applied, leading to $N = 14$ fractions with crack bandwidth $h = 21.21$ mm. In an attempt to simulate the experiment as accurately as possible, Hordijk tension softening [50] is assumed for both cases.

The crack mouth opening displacement (CMOD) is monitored and plotted against the lateral load F for quadrilateral and triangular analyses in Fig. 14 (left) and Fig. 15 (left) respectively. In these figures, two bands of NLFEA solutions are also shown for comparison: (1) the band of results by Ghrib and Tinawi [52], obtained with the aid of both isotropic and anisotropic damage smeared crack formulations, and (2) the band of results by Roth et al. [53] obtained by XFEM analyses with a crack-tracking algorithm. Both studies are based on the same material properties that are used in this study. Furthermore, the experimental results are included as well [51]. The corresponding crack-strain plots for a CMOD of 2 mm for the SLA and fraction model analyses are also found in the Figs. 14, 15 (right (A)–(B)).

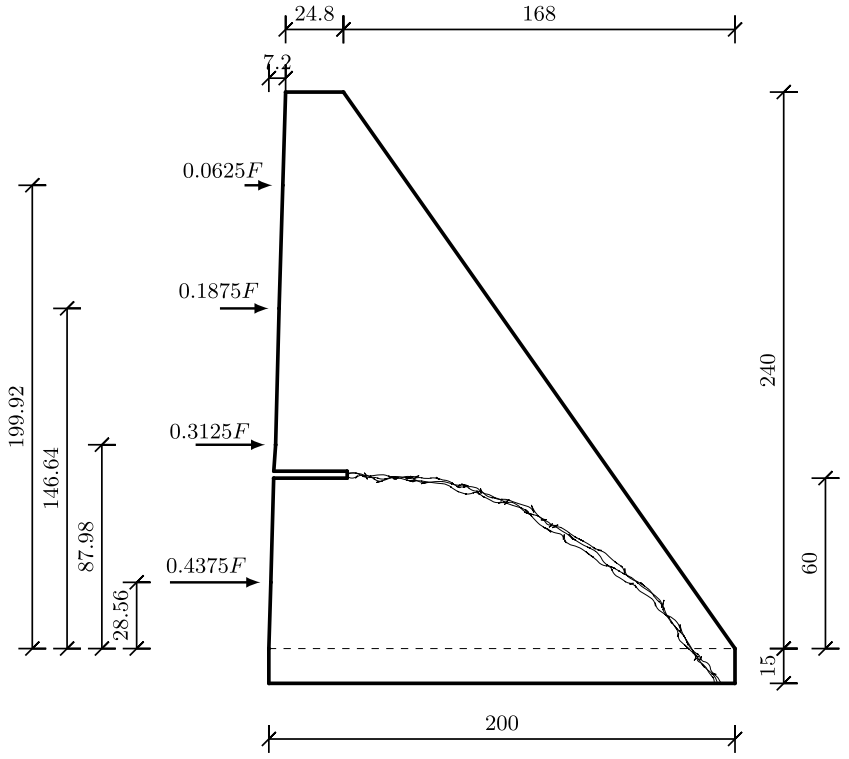

Fig. 13. Geometry of the reduced scale gravity dam with all dimensions in cm.

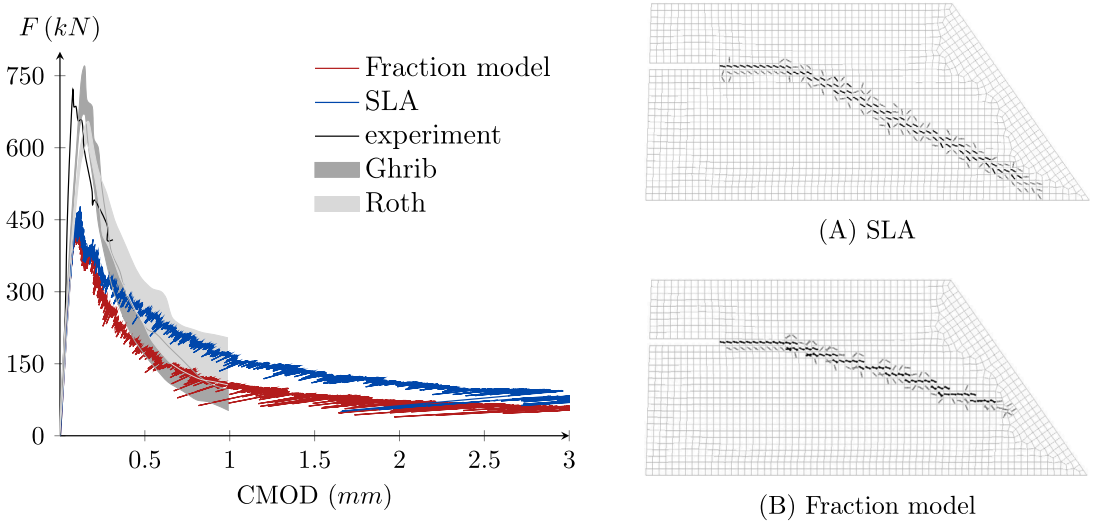

Fig. 14. Load F versus CMOD for the reduced scale gravity dam FE model using quadrilateral elements (left) and crack strain plots (right) for both regular SLA (A) and the fraction model (B) at a crack mouth opening displacement (CMOD) of 2 mm.

For the fine mesh of quadrilaterals, significant differences are obtained between both methods. Regular SLA is able to reach the downstream bottom of the dam, indicating that the influence of mesh-directional bias is reduced when making use of quadratic elements [54]. However, as can be clearly seen in Fig. 14, the fraction model suffers from severe mesh-directional bias and hence, the bottom of the concrete dam is not reached. Apparently, instead of propagating further downwards, the fractions correct the crack direction to maintain mesh alignment. In a study by Bhattacharjee and Léger [43], two types of analyses were performed on the scaled concrete dam: One with a fixed crack model with variable shear retention factor and second a coaxial rotating crack model. Bhattacharjee and Léger concluded that the stress locking that is developed due to a fixed crack direction probably induces

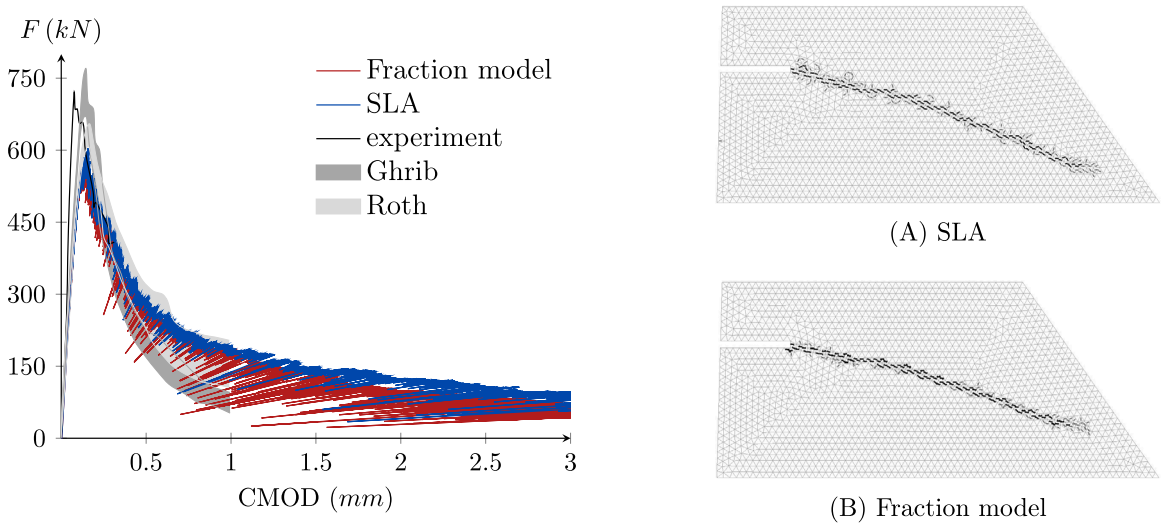

Fig. 15. Load F versus CMOD for the reduced scale gravity dam FE model using triangular elements (left) and crack strain plots (right) for both regular SLA (A) and the fraction model (B) at a crack mouth opening displacement (CMOD) of 2 mm.

high internal forces that are able to overcome issues related to mesh-directional bias. With the aid of a rotating crack model, these high internal forces do not develop since the crack direction is able to correct itself and hence, a straight crack path is obtained (for a very rough mesh). Ghrib and Tinawi [52] came to the same conclusions: the rotating crack model follows the horizontal mesh lines and does not suffice for this case. They advised to make use of a fixed crack model instead. Since the fraction model tries to mimick a rotating crack model, the issues that are encountered for a rotating crack model in the aforementioned works [43,52] are to a certain extent also found for the current fraction model study (possibly less severe issues, since on fraction level, the crack is fixed). In summary, the advantage of the fraction model comes with the disadvantage of possibly having to correct the crack direction to avoid a mesh-directional bias.

Next, the results obtained with triangular elements are presented in Fig. 15. Compared to quadrilateral elements, better agreement with the experimental crack path is found since much less problems related to mesh-directional bias are observed. When comparing the crack paths of regular SLA and the fraction model, less spurious stresses are found in the latter and therefore smaller localisation bands are obtained.

Lastly, the load–CMOD curves of Figs. 14, 15 (left) are discussed. In line with the crack paths, best agreement with experimental results is obtained with triangular elements. Quadrilateral elements result in a lower peak load, which can be possibly attributed to the incorrect crack band assumption: a zig-zag crack path is assumed, while the actual crack path is directed more or less in line with the mesh. All curves reveal that a more flexible response is obtained for the fraction model compared to regular SLA, in line with previous case studies. For triangular elements, the load–CMOD curves of the fraction model better suit the NLFEA solutions of previous works in Refs. [52,53], indicating that the more flexible response is desirable. The curves for quadrilateral elements are difficult to compare: the fraction model gives a more flexible response, but the crack patterns that are found by regular SLA are more correct for these cases.

5.5. 3D: inclined notched beam

Finally, the application of the 3D elastic-brittle fraction model is verified on structural level. In the previous case studies, it has been observed that differences between regular SLA and the fraction model are found for curved crack propagation (e.g. for the shear notched beam in Section 5.3). Therefore, 3D non-planar curved crack propagation is considered in this section with the aid of the skew-notched beam in a three-point bending test. The skew-notched beam has been used by others as a benchmark test to verify 3D (often XFEM related) numerical algorithms [25,55,56]. The geometry, as shown by Fig. 16(left), is in line with the 2D notched beam of Section 5.2, although the notch has a height of only 30 mm and is applied under an angle of 45 degrees, such that the front and rear notches are 60 mm apart. The geometry is taken from the study of Pari et al. [25]. For the purpose of this study, the loading is restricted to a proportional vertical mid-span line load f = F/t, where t = 120 mm, and seems justified, since non-planar crack propagation is also expected for proportional loading. Applied material properties of the specimen are listed in Table 2 and are exactly equal to Section 5.2. Linear tension softening is assumed.

As can be seen in Fig. 16(right), the nonlinear material zone (light grey) with the notch width of 10 mm and element size of 12 mm, and the linear material zone (dark grey) with element size 30 mm is made to reduce computational efforts as against a finer mesh of the same case used previously in the work of Ref. [25]. 4-noded three-side isoparametric solid tetrahedron element with single integration point are applied, such that constant strain distributions are found over the entire element. A ripple band parameter $p = 0.2$ is applied, leading to $N = 12$ fractions with crack bandwidth $h = 6$ mm.

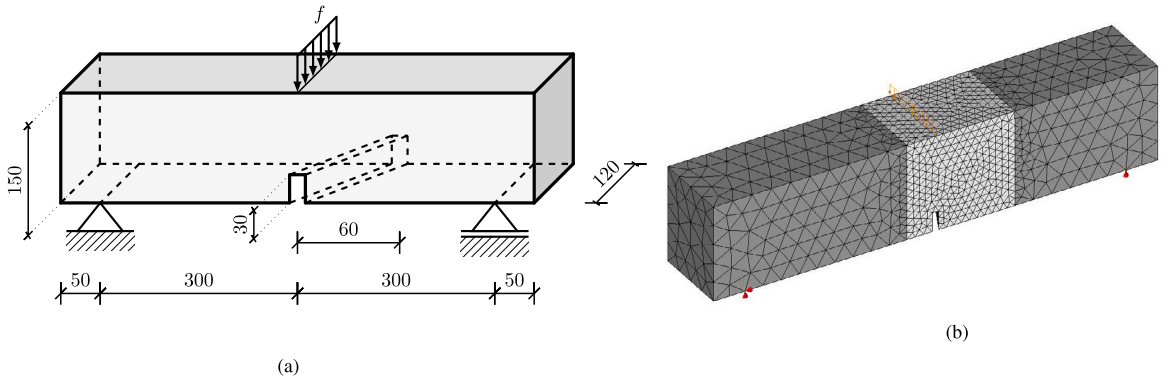

Fig. 16. Geometry of the skew-notched beam in a three-point bending test with all dimensions in mm (left), and the finite element model (right) with nonlinear material behaviour assigned to the light grey area.

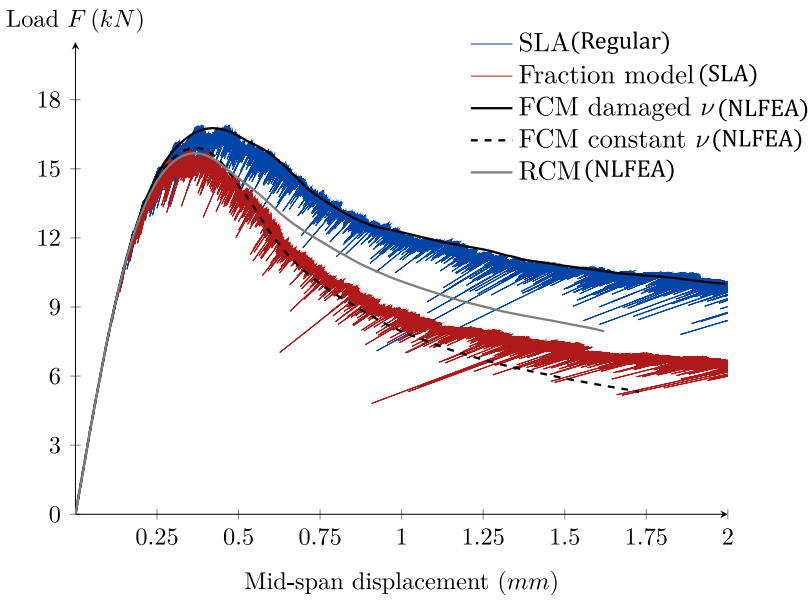

Fig. 17. Load F versus mid-span displacement for the skew-notched beam for regular SLA, the fraction model and NLFEA.

Five types of simulations are run. The first two are with the regular SLA and fraction models, and the rest are all nonlinear finite element analyses (NLFEA). All NLFEA simulations invoke a Newton–Raphson iteration scheme with displacement steps of 0.012 mm and an energy norm of 0.0001 as convergence criteria. The three NLFEA simulations are: (1) NLFEA based on a fixed crack model (FCM) with damage based reduction of the Poisson's ratio and variable shear retention, being the counterpart of regular SLA; (2) NLFEA based on a fixed crack model (FCM) with no damage based reduction of Poisson's ration, such that a constant Poisson's ratio is applied alongside a variable shear retention; (3) NLFEA based on a rotating crack model (RCM) with damage based reduction of Poisson's ratio and shear retention based on the principle of coaxiality.

The force–displacement curves of the simulations are shown in Fig. 17. NLFEA with the fixed crack model and damage based Poisson's ratio and shear reduction shows very good agreement with regular SLA. Considering the second NLFEA case, the constant Poisson's ratio is not in line with the theoretical framework of regular SLA and therefore clear differences are found between both NLFEA and SLA. Since Poisson's ratio is not reduced during damage increments, larger spurious stresses develop within the crack plane, ensuring quicker application of damage increments and therefore, the post-peak load reduces relatively fast as well. In the NLFEA with the rotating crack model, a more flexible response is found compared to regular SLA. The load displacement curve is qualitatively similar to the curve of the fraction model: the same peak load is predicted and both analyses seem to converge to approximately the same load. However, as has already been discussed in previous case studies, the fraction model is not able to exactly match with the rotating crack model due to previously cracked fractions (with outdated crack angles) contributing to the total behaviour. To that end, it is a remarkable finding that the fraction model for this case results in an even more flexible response than the rotating crack model, indicating the presence of even less spurious stresses, where one would contrarily expect a somewhat

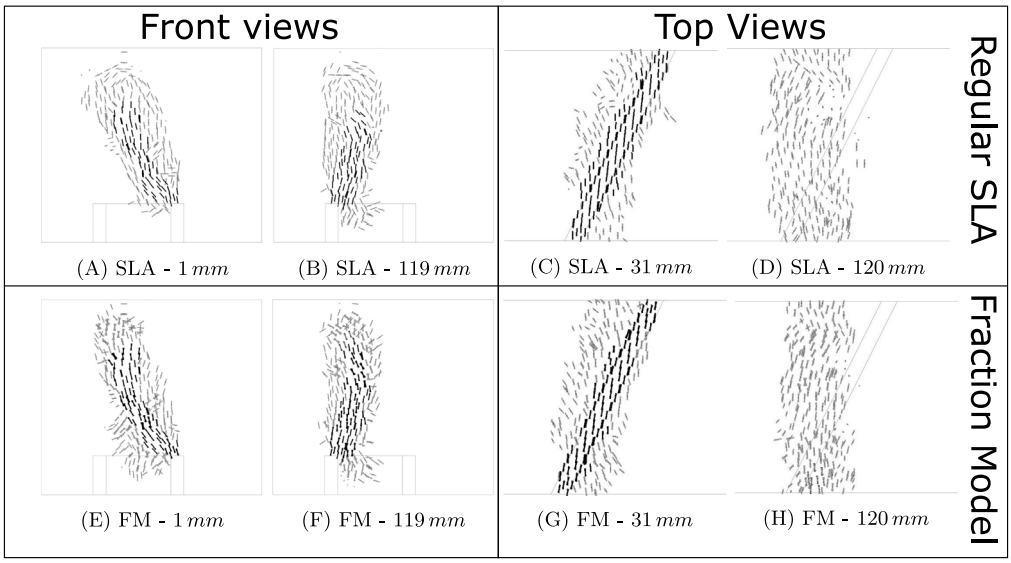

Fig. 18. Crack strain plots in vertical planes at 1 mm and 119 mm from front (0 mm) to rear (120 mm) of the model (i.e Front views A, B, E, F), and Crack strain plots in horizontal planes at 31 mm and 120 mm from bottom (0 mm) to top (150 mm) of the model (i.e Top views C, D, G, H); for regular SLA and the fraction models at a mid-span displacement of 1.2 mm.

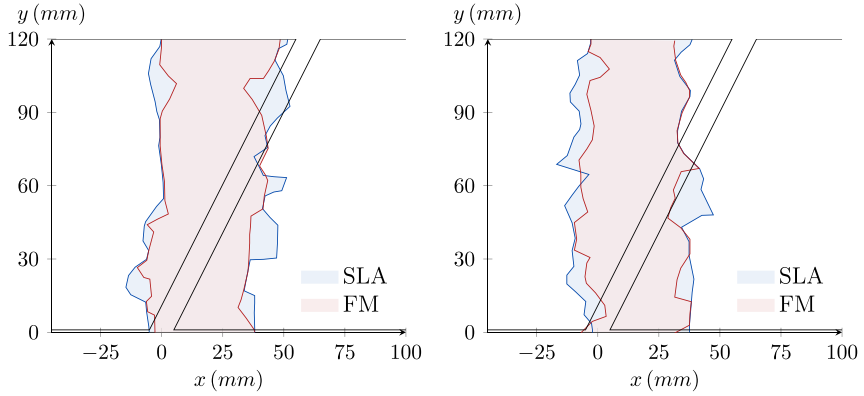

Fig. 19. Comparison of crack paths for regular SLA and fraction models in the horizontal planes 90 mm and 120 mm from the bottom of the FE Model.

stiffer response. This observation is substantiated in the following paragraph. It can however be concluded that better agreement with the rotating crack model is encountered by invoking the 3D implementation of the fraction model as compared to regular SLA.

With the aid of so-called cutting planes, on which all crossed elements project their cracks, crack strain plots are generated from the front side to the rear side and from the bottom to the top in Fig. 18. A curved 3-dimensional crack pattern is observed for both methods. Starting from the front side, the straight vertically directed crack gradually transfers to an inclined curved crack at the rear side of the beam. Furthermore, starting from the bottom side of the beam, the crack gradually straightens towards the top, rotating from the notch direction towards the direction of the line load. In this way, a non-planar 3-dimensional crack path is obtained above the inclined notch. In line with the U-turns that were found for the notched beam of Section 5.2, the crack paths corresponding to regular SLA in Fig. 18 (left) seem to be lost near the top, i.e. the crack directions at the crack tip start to deviate from the direction of crack propagation, such that ultimately, almost horizontally aligned cracks are found at the crack tip. Crack directions in regular SLA are fixed and hence, further crack propagation is arrested near the top. In this way, spurious stresses enforce the crack path to be lost. To correct for this horizontally aligned crack, the fraction model exhibits crack rotations at this location, such that further crack propagation is possible. To this end, further propagated fully developed cracks are observed for the fraction model. Furthermore, slightly bigger bands of spurious stresses near the top are found for regular SLA as a result of the lost crack path. The latter statement is supported by Fig. 18 (right) and Fig. 19 in which differences are found in the width of the

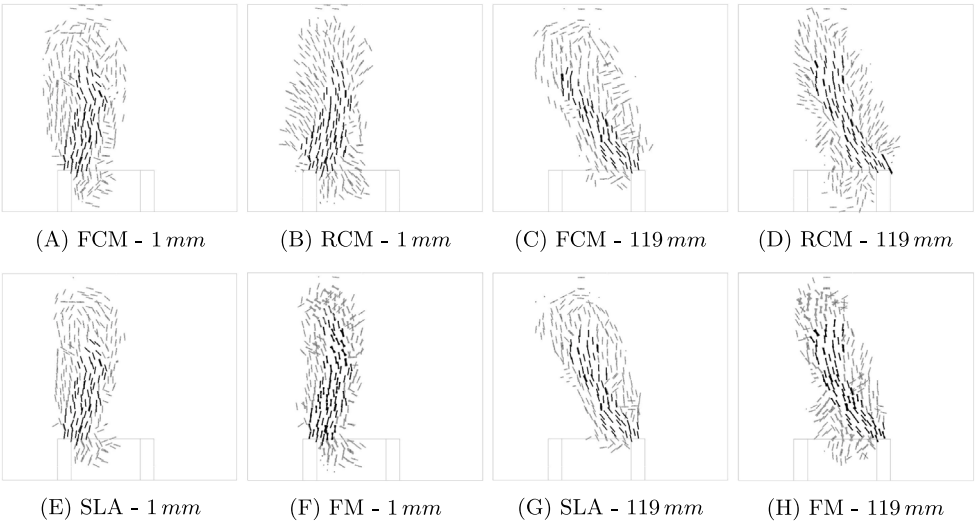

Fig. 20. Comparison of crack paths FCM and RCM NLFEA with regular SLA and the fraction model in vertical planes at 1 and 119 mm from front side for a mid-span displacement of 1.2 mm.

localisation band, especially at height of 90 and 120 mm from bottom. Fig. 19 gives an overlay of the crack paths for these two specific heights. Based on this overlay, it is concluded that the amount of spurious stresses is significantly reduced by the fraction model. Combined with the more correct crack path at the top, this results in a less stiff response with less spurious energy dissipation compared to regular SLA, as can be observed in the load–displacement curve in Fig. 18.

Finally, the crack strain plots of NLFEA fixed crack model (FCM) and regular SLA are very similar as shown in Fig. 20. Although FCM results in a slightly wider localisation band, both exhibit the same main crack path and a U-turn type of behaviour at the top, troubling further crack propagation. The similarity also explains the excellent agreement between the load–displacement curves of FCM and regular SLA. The crack strain plots of NLFEA rotating crack model (RCM) and the fraction model also show similarities. The fully developed crack paths show an almost one-to-one agreement. Also, the additional crack zone next to the notch is similarly captured by both analyses. However, as becomes clear from sub figures (B) and (F) in Fig. 20, RCM results in a wider band of cracks due to spurious stresses compared to the fraction model. Apparently, the SLA-type of procedure restricts the development of spurious crack paths, explaining the even more flexible behaviour that is obtained by the fraction model in the load–displacement curve. A possible cause of this observation might be that for SLA-type of procedures, only a single damage increment is performed at a time, potentially allowing for a certain degree of self-correction in the next steps, while for NLFEA, damage increments are performed in any step anywhere throughout the structure, such that a complete zone of integration points can enter the spurious regime and thus spurious cracks occur simultaneously. To this end, it is less likely for SLA-type of procedures that large zones of spurious stresses develop. Although a more thorough study on the generation of spurious stresses in RCM and FCM would be interesting, especially compared to SLA-type of analyses, such a study is beyond the scope of this article.

6. Discussion

The differences between regular SLA and the fraction model, in general can lead to smoothening of crack paths as observed in all case studies. This is due to the crack rotation on an element level, since the stresses are monitored in a plane that is more in line with the principal stress direction resulting in less over-stiff behaviour. Spurious stresses and cracks, and therefore crack paths, are observed in surrounding elements with regular SLA due to stress locking at the element level. However, the fraction model implicitly allows for correction due to the said flexible behaviour at the element level thereby counteracting the further development of spurious stresses in surrounding elements. In summary, over all case studies more flexible post peak behaviour in the load–displacement responses and sharper localisation bands are obtained with the fraction model which is in line with the structural behaviour. Furthermore, the performance of the fraction model yields some interesting insights which are described in the following.

Comparison with other constitutive models: Rots [2] mentions that fixed smeared cracking approaches are observed to suffer from excessive orthogonal cracking. As a fixed crack is not able to co-rotate with the principal stresses, orthogonal cracking is the only way for an element to ‘compensate’ for the crack direction. This effect is also observed for regular SLA in all case studies. Contrarily, since crack rotation is simulated by the fraction model, the effects of orthogonal secondary cracking are much less pronounced, resulting in a better approximation of the rotating crack as in NLFEA observed in the tension-shear problem (Section 5.1). In the fraction model, shear retention occurs implicitly as a consequence of the rotating crack plane over the different fractions, since previously cracked fractions generate shear stresses not along their cracking planes. Varying β does not lead to a

notable variance of the stress state, indicating that only small shear stresses are found within the cracking planes [54]. As a matter of fact, when comparing the fraction model with the different smeared cracking approaches i.e. fixed/rotating/multi-directional fixed crack, similarities are found with the multi-directional fixed cracking model which allows for multiple cracks to form within one integration point, where the angle between two consecutive cracks is controlled by a threshold angle α. The superposition of fraction cracks can be interpreted as a multi-directional fixed crack. Furthermore, in line with the multi-directional fixed crack model, coaxiality between principal strains and stresses is not maintained for the fraction model. The previously cracked fractions are the reason that the element's principal stress direction does not match the principal strain direction. The model also shows similarities with the approach of Cook et al. [31] which is also a multi-directional crack model with cracking planes, having each their own predefined crack direction. As opposed to the large amount of predefined cracking planes on element level in this approach, each fraction of the fraction model is allowed to crack in any direction, depending on the principal stress direction, and therefore, a wide spectrum of cracks can be simulated without the need to apriori define a large amount of cracking planes. The authors see similarities with the microplane model [35] where tensorial stress strain relations are obtained from stress and strain vectors on planes of various orientations, called microplanes, wherein damage is enforced. But the applicability of the microplane model in the SLA solution framework is to be investigated.

Influence of the mesh: element type, order and integration schemes: Sensitivity studies on the case studies in this article were also carried out, with respect to integration schemes and order/interpolation scheme of the elements [54] which are not presented herein considering constraints on the length of the article. The studies on integration schemes reveal that the influence of spurious stresses is less severe for reduced integration scheme (1-point) or in some cases hardly any [54]. This is because for regular integration schemes like 2×2 or higher, a large part of the area belonging to an integration point closer to an adjacent cracked is subjected to severe straining resulting in spurious stresses. In case of the single-point integration scheme, the spurious behaviour is in fact averaged over the complete element. Furthermore, it was also concluded that using regular 2×2 integration, a non-stable process of increasing asymmetry was initiated and spurious stresses due to incorrect crack directions are formed as a result of asymmetric generation of spurious stresses. This was in-turn was due to the inability of the elements to follow the discontinuous nature of the displacement field. The studies on interpolation schemes reveal that for simple straight crack paths like the notched beam (Section 5.2), linear elements are most suitable, especially when making use of reduced integration. For straight cracks, quadratic elements are too sophisticated and additional spurious stresses are observed. However, quadratic elements are recommended for all curved and diffuse crack paths, since the elements interpolation scheme allows for a more accurate and realistic description of curved crack paths, which becomes especially clear for the shear-notched beam (Section 5.3). As an alternative, linear elements with reduced integration can be used for simple curved crack cases, although the obtained crack path is more or less the collection of piece-wise straight cracks. For the concrete dam cases, linear elements with reduced integration are too simplistic, and no satisfying results can be obtained. Especially for quadratic triangular elements in case of the concrete dam (Section 5.4), mesh-directional bias was observed to reduce, although the issues are not completely solved. Potentially, the influence of mesh-directional bias can be reduced by using random triangular meshes. Further research is required to substantiate the latter statement. It can however be concluded that quadratic-order elements, triangular or quadrilateral, could yield asymmetric and localised cracks within elements suitable for some specific cases but linear elements would be best suited for application in engineering practice for larger cases due to the constant strain distribution within the element. With the aid of the fraction model, the general performance of different elements relatively to each other does not change, and in general, element-related issues are maintained. Furthermore, mesh sensitivity is indeed an important aspect, as the fraction model is based on the total strain based smeared cracking approach. It has previously been shown that results are mesh objective with regular fixed crack SLA [13] and this is expected to follow in the fraction model as well. However, this aspect has not been investigated in this work. The mesh directional bias is indeed an issue as is observed in the case studies presented herein.

Crack direction tracking: In the delayed crack path fixation approach of Slobbe et al. [21], the crack-path is fixed once a certain amount of damage has taken place. In this way, the occurrence of U-turns as shown in Fig. 10 is resolved. Following this line of thinking, the fraction model can in fact also be seen as a type of delayed crack path fixation, since the crack path direction is not directly fixed after initiation, but is gradually fixed once damage increases and more fractions are cracked, which can be interpreted as a 'delayed' type of crack path fixation.

Events and snap-backs: Furthermore, when looking in more detail to force–displacement curves, it is to be noted that the snaps herein are not the global snap-back type equilibrium paths but rather the load-unload type spikes typical of SLA. In order to understand this difference, it is first explained why snap-backs occur for regular SLA [18,57,58]. Stress jumps occur when multiple neighbouring elements are almost loaded up to their tensile strength. In this case, a damage increment can only be performed for the most critical integration point, after which a stress distribution takes place that relieves the critical integration point. The surrounding elements are not able to take over the released stress and the only way to distribute these stresses is by reducing the load factor, thereby causing a snap-back. This process is repeated several times until the surrounding elements allow for recovery of the load factor. The large snapbacks of both regular SLA and the fraction model are found at roughly the same places in the load-displacement curves, meaning that the underlying cause for snap-backs is the same for the fraction model. However, the snap-backs are bigger for the fraction model compared to regular SLA, which is most likely the result of a fundamental difference between the two models. For regular SLA, the critical integration points are often already cracked and therefore considered in the fixed crack direction, meaning that not by definition the direction with the highest stresses is monitored. For the fraction model with brittle damage increments, the critical fraction is most often uncracked (except for perpendicular cracking) and stresses are considered in the maximum direction. As a result, the monitored stresses in the surrounding elements are potentially closer to the tensile strength for the fraction model, since regular SLA does not monitor the stresses in the surrounding elements in the maximum direction.

Since the surrounding elements have higher stresses, the released stress after a damage increment becomes even more difficult to distribute and the loading should be reduced even further, causing bigger snap-backs to occur for the fraction model compared to regular SLA.

Moreover, the results in SLA i.e. the load–displacement curves are dependent on the fineness of the saw-tooth law. In other words, more the number of secant branches in the material law, smoother the force–displacement response and equivalent to a nonlinear analysis with the regular constitutive law [13,19]. Since the fraction model draws its characteristics from these saw-tooth laws in SLA, it can be extended that more the number of fractions, a smoother force–displacement response would be expected.

7. Conclusions and outlook

In this article, the framework of regular sequentially linear analysis (SLA) has been extended towards the fraction model (both 2D and 3D), which subdivides each element into a parallel set of elastic-perfectly brittle fractions, each having their own Young's modulus, strength and fixed crack direction. The superposition of fractions, in an overall sense, results in a rotating crack on element level and therefore, the fraction model is observed to mimick a rotating crack. It represents the progressive loss of cross section in how the micro-cracking eventually leads to macro cracking, resulting in a more realistic description of damage propagation in quasi-brittle concrete structures.

A single element case and 4 structural case studies have been presented herein, illustrating the performance of the fraction model in comparison to regular SLA (using the fixed crack approach) and additionally, some NLFEA. It has been consistently shown that the fraction model is better able to approximate a rotating crack model compared to regular fixed crack SLA, such that the effects of stress locking are reduced, less wide bands of spurious stresses are obtained around the main crack path leading to less energy dissipation; and therefore, more flexible post-peak responses are observed.

Some improvements to the fraction model, i.e a tapered ripple band formulation, tension-compression interaction effects for both primary and secondary crack initiation, and crack-closure have been proposed already [54]. These extensions would further improve the model in its applications in the realm of concrete structures. It is also recommended to perform a variation study to further understand and optimise the selection of the ripple band parameter p. It might be useful to develop guidelines that describe the relation between the ripple band parameter and the obtained level of accuracy. Also, further research is recommended on how to reduce issues related to mesh-directional bias for the fraction model. Throughout this study, it has been consistently observed that the crack path tried to follow the mesh lines, which became especially prevailing for linear quadrilateral elements with regular integration. Potentially, random triangular meshes might reduce these effects. On top of that, the fraction model can be combined with crack tracking algorithms, in line with the works of Slobbe [21] and Cook et al. [31], within the framework of regular SLA. With regard to the presented 3D case study, although the results are very promising and in line with the findings of the 2D cases, the computation efforts that come along with SLA-type of procedures for 3D problems are a drawback. On top of that, additional computational efforts are required for the fraction model, in which multiple overlay volume elements are applied. Although the current theoretical framework of the fraction model is restricted to 2D membrane and 3D solid elements, application to shell elements is also possible following the same principles as discussed in this article—extending on work of DeJong for SLA with shell elements [24].

With regard to the sequentially linear approach in general, several extensions can still be made to extend its applicability mainly in relation to loading or stress history related nonlinear problems. The approach is currently being used for monotonic applications, but cyclic loading studies are possible in an incremental approach with non-secant saw-tooth laws [58], in conjunction with a stress-reversal algorithm [54,58]. The approach also needs to be extended to large-deformation applications i.e for geometric nonlinear cases. Furthermore, the suitability of the incremental sequentially linear approaches for plasticity rather than brittle problems needs investigation.

CRediT authorship contribution statement

D. Bresser: Writing – original draft, Visualization, Validation, Software, Methodology, Investigation, Conceptualization. **J.G. Rots:** Writing – review & editing, Supervision, Funding acquisition, Conceptualization. **M.A.N. Hendriks:** Review & editing, Supervision, Conceptualization. **M. Pari:** Review & editing, Writing – original draft, Supervision, Software.

Declaration of competing interest

The authors declare that they have no known competing financial interests or personal relationships that could have appeared to influence the work reported in this paper.

Data availability

Data will be made available on request.

Acknowledgements

The implementation of the presented concepts was carried out in the commercial package DIANA and the authors are thankful for the collaboration with DIANA FEA B.V. towards the development of SLA and the forthcoming new implementations in this topic

References

[1] Gu X, Jin X, Zhou Y. Basic principles of concrete structures. Springer-Verlag Berlin Heidelberg; 2016, http://dx.doi.org/10.1007/978-3-662-48565-1.
[2] Rots JG. Computational modeling of concrete fracture [Ph.D. dissertation], Delft University of Technology; 1988.
[3] de Borst R, Crisfield MA, Remmers J, Verhoosel C. Non-linear finite element analysis of solids and structures. 2nd ed. Chichester: Wiley; 2012, http://dx.doi.org/10.1002/9781118375938.
[4] Hendriks MAN, Rots JG. Sequentially linear versus nonlinear analysis of RC structures. Eng Comput 2013;30(6):792–801. http://dx.doi.org/10.1108/EC-May-2012-0105.
[5] Rashid YR. Ultimate strength analysis of prestressed concrete pressure vessels. Nucl Eng Des 1968;7(4):334–44. http://dx.doi.org/10.1016/0029-5493(68)90066-6.
[6] Bažant ZP, Oh B. Crack band theory for fracture of concrete. Matér Constr 1983;16:155–77. http://dx.doi.org/10.1007/BF02486267.
[7] Wempner GA. Discrete approximations related to nonlinear theories of solids. Int J Solids Struct 1971;7(11):1581–99. http://dx.doi.org/10.1016/0020-7683(71)90038-2.
[8] Verhoosel CV, Remmers JJC, Gutiérrez MA. A dissipation-based arc-length method for robust simulation of brittle and ductile failure. Internat J Numer Methods Engrg 2009;77(9):1290–321. http://dx.doi.org/10.1002/nme.2447.
[9] Herrmann HJ, Hansen A, Roux S. Fracture of disordered, elastic lattices in two dimensions. Phys Rev B 1989;39:637–48. http://dx.doi.org/10.1103/PhysRevB.39.637.
[10] Schlangen HEJG. Experimental and numerical analysis of fracture processes in concrete [Ph.D. dissertation], Delft University of Technology; 1980.
[11] Beranek WJ, Hobbelman GJ. 2D and 3D-modelling of concrete as an assemblage of spheres: revaluation of the failure criterion. In: Wittmann FH, editor. Proceedings of the second international conference on fracture mechanics of concrete structures. 1995, p. 965–78.
[12] Rots JG. Sequentially linear continuum model for concrete fracture. In: de Borst R, Mazars J, Pijaudier-Cabot G, van Mier JGM, editors. Fourth international conference on fracture mechanics of concrete and concrete structures. vol. 2, Lisse: Swets & Zeitlinger; 2001, p. 831–9.
[13] Rots JG, Invernizzi S. Regularized sequentially linear saw-tooth softening model. Int J Numer Anal Methods Geomech 2004;28(7–8):821–56. http://dx.doi.org/10.1002/nag.371.
[14] Rots JG, Belletti B, Invernizzi S. Robust modeling of RC structures with an event-by-event strategy. In: International conference of crack paths. Eng Fract Mech 2008;75(3):590–614. http://dx.doi.org/10.1016/j.engfracmech.2007.03.027.
[15] Giardina G, van de Graaf AV, Hendriks MAN, Rots JG, Marini A. Numerical analysis of a masonry façade subject to tunnelling-induced settlements. Eng Struct 2013;54:234–47. http://dx.doi.org/10.1016/j.engstruct.2013.03.055.
[16] Invernizzi S, Trovato D, Hendriks MAN, van de Graaf AV. Sequentially linear modelling of local snap-back in extremely brittle structures. Eng Struct 2011;33(5):1617–25. http://dx.doi.org/10.1016/j.engstruct.2011.01.031.
[17] DeJong MJ, Hendriks MAN, Rots JG. Sequentially linear analysis of fracture under non-proportional loading. Eng Fract Mech 2008;75(18):5042–56. http://dx.doi.org/10.1016/j.engfracmech.2008.07.003.
[18] van de Graaf AV. Sequentially linear analysis for simulating brittle failure [Ph.D. thesis, Ph.D. dissertation], Delft University of Technology; 2017, http://dx.doi.org/10.4233/uuid:dd9ea945-136c-4b74-bae2-f1a8cf9a6ed9.
[19] Alfaiate J, Sluys LJ. On the use of non-iterative methods in cohesive fracture. Int J Fract 2018;210(1):167–86. http://dx.doi.org/10.1007/s10704-018-0270-2.
[20] Eliáš J, Frantík P, Vořechovský M. Improved sequentially linear solution procedure. Eng Fract Mech 2010;77(12):2263–76. http://dx.doi.org/10.1016/j.engfracmech.2010.05.018.
[21] Slobbe AT, Hendriks MAN, Rots JG. Smoothing the propagation of smeared cracks. Eng Fract Mech 2014;132:147–68. http://dx.doi.org/10.1016/j.engfracmech.2014.10.020.
[22] Pari M, Van de Graaf AV, Hendriks MAN, Rots JG. A multi-surface interface model for sequentially linear methods to analyse masonry structures. Eng Struct 2021;238:112123. http://dx.doi.org/10.1016/j.engstruct.2021.112123.
[23] Yu C, Hoogenboom PCJ, Rots JG. Incremental sequentially linear analysis to control failure for quasi-brittle materials and structures including non-proportional loading. Eng Fract Mech 2018;202:332–49. http://dx.doi.org/10.1016/j.engfracmech.2018.07.036.
[24] DeJong MJ, Belletti B, Hendriks MAN, Rots JG. Shell elements for sequentially linear analysis: Lateral failure of masonry structures. Eng Struct 2009;31(7):1382–92. http://dx.doi.org/10.1016/j.engstruct.2009.02.007.
[25] Pari M, Hendriks MAN, Rots JG. Non-proportional loading in sequentially linear analysis for 3D stress states. Internat J Numer Methods Engrg 2019;119(6):506–31. http://dx.doi.org/10.1002/nme.6060.
[26] Pari M, Swart W, van Gijzen MB, Hendriks MAN, Rots JG. Two solution strategies to improve the computational performance of sequentially linear analysis for quasi-brittle structures. Internat J Numer Methods Engrg 2020;121(10):2128–46. http://dx.doi.org/10.1002/nme.6302.
[27] Vorel J, Boshoff WP. Computational modelling of real structures made of strain-hardening cement-based composites. Appl Math Comput 2015;267:562–70. http://dx.doi.org/10.1016/j.amc.2015.01.056.
[28] de Putter A, Hendriks MAN, Rots JG, Yang Y, Engen M, van den Bos AA. Quantification of the resistance modeling uncertainty of 19 alternative 2d nonlinear finite element approaches benchmarked against 101 experiments on reinforced concrete beams. Struct Concr 2022;1–15. http://dx.doi.org/10.1002/suco.202100574.
[29] Hendriks MAN, Rots JG. Elastic-brittle fraction model for concrete and masonry structures. In: Bicanic N, Mang H, Meschke G, de Borst R, editors. Computational modelling of concrete structures: proceedings of EURO-C 2014. Leiden: CRC Press/Balkema; 2014, p. 495–503.
[30] Hillerborg A, Modéer M, Petersson PE. Analysis of crack formation and crack growth in concrete by means of fracture mechanics and finite elements. Cem Concr Res 1976;6(6):773–81. http://dx.doi.org/10.1016/0008-8846(76)90007-7.
[31] Cook AC, Vel SS, Johnson SE. Pervasive cracking of heterogeneous brittle materials using a multi-directional smeared crack band model. Int J Mech Sci 2018;149:459–74. http://dx.doi.org/10.1016/j.ijmecsci.2017.09.016.
[32] Jirásek M, Zimmermann T. Analysis of rotating crack model. J Eng Mech 1998;124(8):842–51. http://dx.doi.org/10.1061/(ASCE)0733-9399(1998)124:8(842).
[33] Slobbe AT. Sequentially linear analysis of shear critical reinforced concrete beams [Master's thesis], Delft University of Technology; 2010.
[34] Liu J. Simulating quasi-brittle failures including damage-induced softening based on the mechanism of stress redistribution. Appl Math Model 2018;55:685–97. http://dx.doi.org/10.1016/j.apm.2017.11.014.
[35] Carol I, Bazant ZP. Damage and plasticity in microplane theory. Int J Solids Struct 1997;34(29):3807–35.
[36] Bažant ZP, Lin F. Nonlocal smeared cracking model for concrete fracture. J Struct Eng 1988;114(11):2493–510. http://dx.doi.org/10.1061/(ASCE)0733-9445(1988)114:11(2493).
[37] Voormeeren LO. Extension and verifcation of sequentially linear analysis to solid elements [Master's thesis], Delft University of Technology; 2011.
[38] Willam K, Pramono E, Sture S. Fundamental issues of smeared crack models. In: Fracture of concrete and rock. Springer; 1989, p. 142–57.
[39] Kwon SH, Zhao Z, Shah SP. Effect of specimen size on fracture energy and softening curve of concrete: Part II. inverse analysis and softening curve. Cem Concr Res 2008;38(8):1061–9. http://dx.doi.org/10.1016/j.cemconres.2008.03.014.

[40] Zhao Z, Kwon SH, Shah SP. Effect of specimen size on fracture energy and softening curve of concrete: Part I. experiments and fracture energy. Cem Concr Res 2008;38(8):1049–60. http://dx.doi.org/10.1016/j.cemconres.2008.03.017.
[41] Rots JG, Invernizzi S, Belleti B, Hendriks MAN. Circumventing bifurcations in structural softening. In: Workshop on computational modeling on concrete, masrony and fiber-reinforced composites. Delft University of Technology; 2009.
[42] Slobbe AT. Propagation and band width of smeared cracks [Ph.D. thesis, Ph.D dissertation], Delft University of Technology; 2015, http://dx.doi.org/10.4233/uuid:6c5cbe8e-89a8-460d-857f-c3403789fec4.
[43] Bhattacharjee SS, Léger P. Application of NLFM models to predict cracking in concrete gravity dams. J Struct Eng 1994;120(4):1255–71. http://dx.doi.org/10.1061/(ASCE)0733-9445(1994)120:4(1255).
[44] Cendón D, Gálvez J, Elices M, Planas J. Modelling the fracture of concrete under mixed loading. Int J Fract 2000;103(3):293–310.
[45] Ožbolt J, Reinhardt H. Numerical study of mixed-mode fracture in concrete. Int J Fract 2002;118(2):145–62.
[46] Jirásek M, Grassl P. Evaluation of directional mesh bias in concrete fracture simulations using continuum damage models. Eng Fract Mech 2008;75(8):1921–43. http://dx.doi.org/10.1016/j.engfracmech.2007.11.010.
[47] b. Li J, Gao X, a. Fu X, Wu C, Lin G. A nonlinear crack model for concrete structure based on an extended scaled boundary finite element method. Appl Sci 2018;8(7). http://dx.doi.org/10.3390/app8071067.
[48] Arrea M, A.R Ingraffea. Mixed-mode crack propagation in mortar and concrete. Report No. 81-13; Dept. Struct. Engg, Cornell University Ithaka 1982.
[49] Rots JG, de Borst R. Analysis of mixed & mode fracture in concrete. J Eng Mech 1987;113(11):1739–58. http://dx.doi.org/10.1061/(ASCE)0733-9399(1987)113:11(1739).
[50] Cornelissen H, Hordijk D, Reinhardt H. Experimental determination of crack softening characteristics of normalweight and lightweight. Heron 1986;31(2):45–6.
[51] Carpinteri A, Valente S, Ferrara G, Imperato L. Experimental and numerical fracture modelling of a gravity dam. Fract Mech Concr Struct 1992;351–60.
[52] Ghrib F, Tinawi R. Nonlinear behavior of concrete dams using damage mechanics. J Eng Mech 1995;121(4):513–27. http://dx.doi.org/10.1061/(ASCE)0733-9399(1995)121:4(513).
[53] Roth S-N, Léger P, Soulaïmani A. A combined XFEM–damage mechanics approach for concrete crack propagation. Comput Methods Appl Mech Engrg 2015;283:923–55. http://dx.doi.org/10.1016/j.cma.2014.10.043.
[54] Bresser D. Mimicking a rotating crack model within sequentially linear analysis using an elastic-perfectly brittle sublayer model [Master's thesis], Delft University of Technology; 2019.
[55] Colombo D. An implicit geometrical approach to level sets update for 3D non planar X-FEM crack propagation. Comput Methods Appl Mech Engrg 2012;237–240:39–50. http://dx.doi.org/10.1016/j.cma.2012.04.020.
[56] Jäger P, Steinmann P, Kuhl E. Modeling three-dimensional crack propagation—a comparison of crack path tracking strategies. Internat J Numer Methods Engrg 2008;76(9):1328–52. http://dx.doi.org/10.1002/nme.2353.
[57] Pari M, Hendriks MAN, Rots JG. Non-proportional loading in sequentially linear solution procedures for quasi-brittle fracture: A comparison and perspective on the mechanism of stress redistribution. Eng Fract Mech 2020;230:106960. http://dx.doi.org/10.1016/j.engfracmech.2020.106960.
[58] Pari M. Simulating quasi-brittle failure in structures using sequentially linear methods: studies on non-proportional loading, constitutive modelling, and computational efficiency [Ph.D. thesis, Ph.D. dissertation], Delft University of Technology; 2020, http://dx.doi.org/10.4233/uuid:ca17d04d-4c40-4856-97cd-8808ac641007.